





Anatomical description and systematics of a new notosuchian (Mesoeucrocodylia; Crocodyliformes) from the Quiricó Formation, Lower Cretaceous, Sanfranciscana Basin, Brazil

Joyce Celerino de Carvalho, Daniel Martins dos Santos, Ricardo Lourenço Pinto & Rodrigo Miloni Santucci


To cite this article: Joyce Celerino de Carvalho, Daniel Martins dos Santos, Ricardo Lourenço Pinto & Rodrigo Miloni Santucci (18 Feb 2025): Anatomical description and systematics of a new notosuchian (Mesoeucrocodylia; Crocodyliformes) from the Quiricó Formation, Lower Cretaceous, Sanfranciscana Basin, Brazil, Journal of Vertebrate Paleontology, DOI: [10.1080/02724634.2025.2452947](https://doi.org/10.1080/02724634.2025.2452947)

To link to this article: <https://doi.org/10.1080/02724634.2025.2452947>

 View supplementary material 

 Published online: 18 Feb 2025.

 Submit your article to this journal 

 Article views: 148

 View related articles 

 View Crossmark data 

ANATOMICAL DESCRIPTION AND SYSTEMATICS OF A NEW NOTOSUCHIAN (MESOEUCROCODYLIA; CROCODYLIFORMES) FROM THE QUIRICÓ FORMATION, LOWER CRETACEOUS, SANFRANCISCANA BASIN, BRAZIL

JOYCE CELERINO DE CARVALHO, ¹ DANIEL MARTINS DOS SANTOS, ² RICARDO LOURENÇO PINTO, ³ and RODRIGO MILONI SANTUCCI ^{4*}

¹University of Brasília, Institute of Geosciences, Campus Darcy Ribeiro, Brasília, DF, Brazil, joyce.celerino@gmail.com;

²University of Brasília, Institute of Biological Sciences, Brasília, DF, Brazil, danielmartinsantos@hotmail.com;

³University of Brasília, Institute of Geosciences, Campus Darcy Ribeiro, Brasília, DF, Brazil, rpinto@gmail.com;

⁴University of Brasília, Planaltina Campus (FUP), DF, Brazil, rodrigoms@unb.br

ABSTRACT—Notosuchians comprise a clade of mostly terrestrial crocodyliforms generally found in Cretaceous Gondwanan deposits. They evolved into many forms and some species show convergences with mammalian features such as the development of a high degree of heterodonty and multicuspid teeth. South American deposits concentrate the highest number of described notosuchian species, which is more than twice the number of taxa known from strata elsewhere. Here, a novel candidodontid notosuchian, *Thilastikosuchus scutoeangularis*, gen. et sp. nov., is presented and described, comprising a new monospecific genus and the oldest notosuchian record found in Brazil, and likely from South America. This new taxon lacks the sharp hypertrophied caniniform teeth of closely related forms, such as *Malawisuchus* and *Pakasuchus*, but shares the posterior molariform teeth with increasingly wider crowns and denticulated cingula. Additionally, the phylogenetic analysis with the inclusion of the new Brazilian material places Candidodontidae as the earliest notosuchian radiation, shedding new light into its origins.

<http://zoobank.org/urn:lsid:zoobank.org:pub:8D1D5024-1737-4F0B-BC03-C93291934FCB>

SUPPLEMENTARY FILES—Supplementary files are available for this article for free at www.tandfonline.com/UJVP.

Citation for this article: Celerino de Carvalho, J., Martins dos Santos, D., Pinto, R. L., & Santucci, R. M. (2025) Anatomical description and systematics of a new notosuchian (Mesoeucrocodylia; Crocodyliformes) from the Quiricó Formation, Lower Cretaceous, Sanfranciscana Basin, Brazil. *Journal of Vertebrate Paleontology*. <https://doi.org/10.1080/02724634.2025.2452947>

Submitted: March 22, 2024

Revisions received: December 23, 2024

Accepted: December 24, 2024

INTRODUCTION

Candidodontidae is a group of small-bodied and highly heterodont notosuchians, so far restricted to Lower Cretaceous deposits of Gondwana (Africa and South America), and first suggested to comprise a clade by Carvalho et al. (2004). According to the latest phylogeny focused on Candidodontidae (Martin & Borin, 2016), it is currently represented by the following species: *Candidodon itapecuruense* Carvalho 1994; *Lavocatchampsa sigogneaurussellae* Martin & Broin, 2016; *Malawisuchus mwakasyungutiensis* Gomani 1997; and *Pakasuchus kapilimai* O'Connor et al., 2010. The clade was initially defined by Carvalho et al. (2004) as the most recent common ancestor of *Candidodon* and *Mariliasuchus*, and all its descendants. Montefeltro et al. (2009) proposed a new phylogenetic definition for the clade, defining it as all forms more closely related to *Candidodon* and *Mariliasuchus* than to other notosuchians and crocodylians like *Notosuchus terrestris*, *Sphaesaurus huenei*, *Baurusuchus pachecoi*, and *Crocodylus niloticus*. Nonetheless, Martin and De Broin (2016) provided a new diagnosis for Candidodontidae

as small notosuchians with short and triangular rostra, relatively large molariforms, and cingulated teeth with accessory cusps surrounding complex crowns. While being formerly and subsequently recovered as a monophyletic group (e.g., Bravo et al., 2021; Carvalho et al., 2004; Martin & De Broin, 2016), other topologies, despite being based on the same dataset, reject its monophyly, such as Pol et al. (2012, 2014), Leardi et al. (2015a), Fiorelli et al. (2016), and Martinelli et al. (2018).

A new species, inferred to belong to Candidodontidae, is presented here (FUP-Pv-000019). This material, recovered from Lower Cretaceous outcrops of the Sanfranciscana Basin, northern Minas Gerais State, Brazil, likely represents the oldest (alongside *Amargosuchus minor* Chiappe, 1988) and one of the most complete South American notosuchians known to date. Besides, this new candidodontid notosuchian is the first crocodyliform taxon to be formally described for the Sanfranciscana Basin, a relatively new paleontological frontier that has been broadening the scope of South American Lower Cretaceous tetrapod diversity, with significant recent vertebrate discoveries (e.g., Bittencourt et al., 2020; Carvalho & Santucci, 2018, 2021, 2023; Zaher et al., 2011, 2020). The specimen is well preserved and relatively complete, being partially articulated and found in close association with other fossil occurrences, such as gastropods, Lepisosteidae and sarcopterygian fish

*Corresponding author.

Color versions of one or more of the figures in the article can be found online at www.tandfonline.com/ujvp.

remains, lizards, as well as sauropod and theropod dinosaurs (Carvalho & Santucci, 2018, 2021, 2023).

Computed tomography was applied to assist in-depth anatomical descriptions and consequently allowed for the digital articulation of appendicular elements, improving character codification. Moreover, the character states of all members of Candidodontidae were revised, and the inclusion of a new species resulted in a new topology with relevant implications for the understanding of notosuchian radiation.

Regional Geological Context

The Sanfranciscana Basin partially covers the São Francisco Craton and spreads along the states of Minas Gerais, Goiás, Bahia, and Piauí, occupying an area of nearly 150,000 km² (Batezelli et al., 2024). It is mostly composed of continental deposits ranging from the Paleozoic to more recent Cenozoic strata (Campos & Dardenne, 1997a and b). The most fossil-rich unit is the Quiricó Formation, yielding gastropod shells, crustaceans, fish, lizards, and dinosaurs (Bittencourt et al., 2018, 2020; Carvalho & Meisey, 2008; Carvalho & Santucci, 2018, 2021, 2023; Zaher et al., 2011, 2020). It is considered as representing a lacustrine system with localized low-density turbidite deposits (Campos & Dardenne, 1997a; Carvalho & Kattah, 1998).

Age estimates for the Quiricó Formation are all based on microfossil biozones and mostly converged, with one exception. Lima (1979) inferred a Barremian age considering palynomorph data corresponding to the *Trasitoripollis crisopolensis* zone. Arai et al. (1995), also based on palynomorphs, corroborated a Barremian estimate, but highlighted that top-sequence shales would likely be younger due to the presence of *Afropollis* grains. Freshwater ostracods, recovered from the lowest levels, also point to a Barremian age (Carmo et al., 2004). Nevertheless, Leite et al. (2018), describing new ostracod assemblages, defended a Valanginian age interval for the Quiricó Formation, later being questioned by Coimbra (2020), who considered it as an assemblage comprised of endemic novel taxa and, therefore, showing limited biostratigraphic value.

The crocodylomorph material herein described was collected within massive red sandstones, located directly above its contact with lower, alternating layers of fine sandstone and mudstones with parallel lamination which are traditionally attributed to the Quiricó Formation. Distinct ripple marks and desiccation cracks are present near the collecting point, indicating that these rocks represent shallow water deposits near the margin of the Quiricó lake. Surrounding sediments also produced several gastropods and fish remains. According to Cabral et al. (2021), the upper horizons of the Quiricó

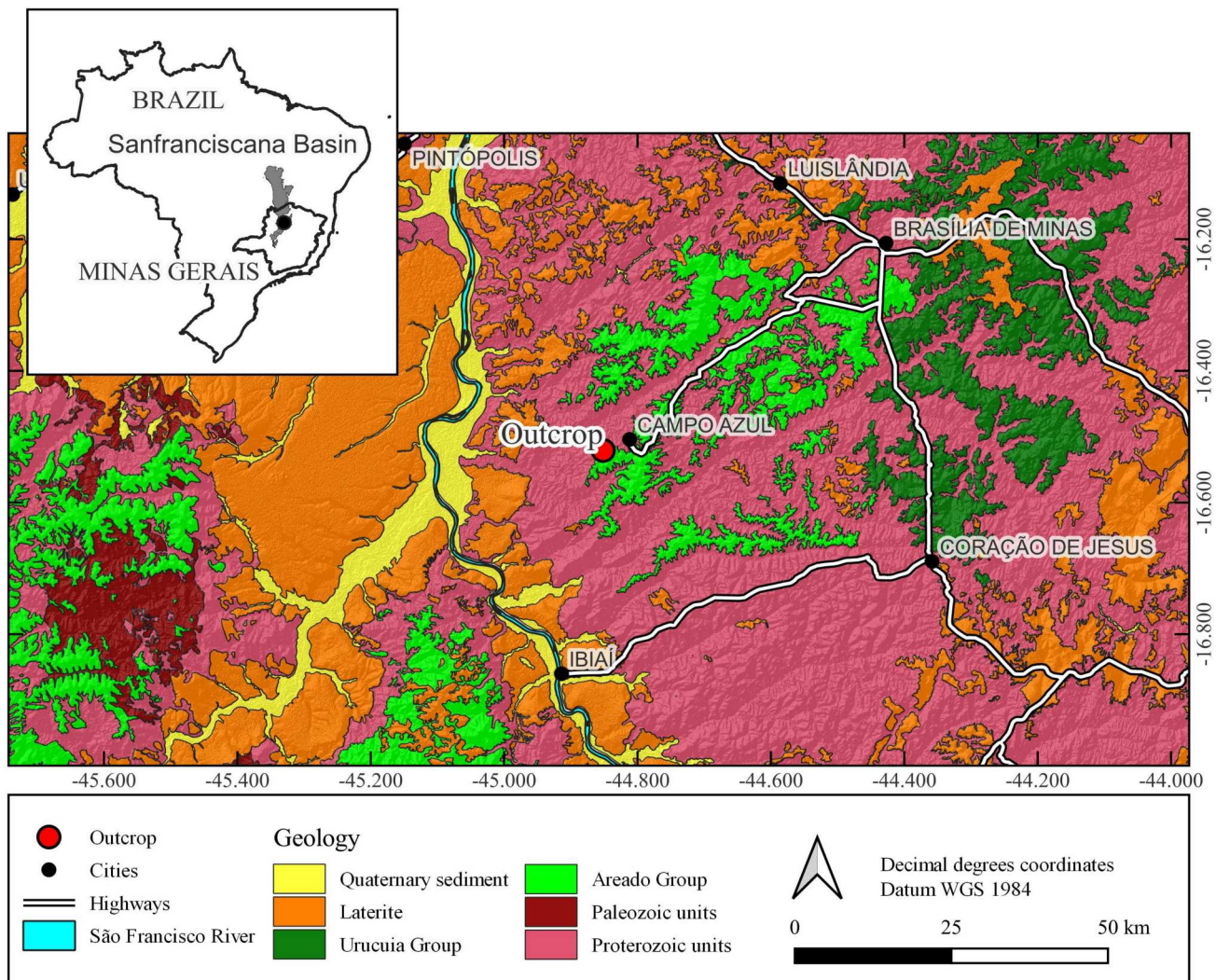


FIGURE 1. Collecting site and geological map of the Sanfranciscana Basin. The city of Campo Azul, Minas Gerais State, is represented by a black circle.

Formation show increasing interaction with other depositional systems, especially with the fluvial-eolian lower facies of the Três Barras Formation that must have covered the Quiricó lacustrine deposits. Given the above-mentioned geological context, a mid-sequence position within the Quiricó Formation was inferred for the material reported here.

MATERIALS AND METHODS

The fossil was collected in the Campo Azul municipality (Fig. 1), Minas Gerais State (Brazil), and subsequently housed in the vertebrate paleontology collection of the University of Brasília (UnB)—Planaltina Campus under the reference number FUP-Pv 000019.

Computed Tomography

Skull and appendicular elements were digitized at a micro-metric scale using the Zeiss Xradia Versa XRM-510 X-ray microtomograph at the Technological Characterization Laboratory of the University of São Paulo. Both the cranium and mandibles were scanned, in addition to a complete right anterior autopodium. The images were at a slice resolution of 0.05 mm, using a voltage of 100 kV with an intensity of 70 mA, and 1000 projections. The resulting images were processed using ITK-SNAP software (Yushkevich et al., 2006). CT scans are deposited in the digital repository Zenodo and can be accessed at <https://doi.org/10.5281/zenodo.13357095>.

Cladistic Analysis

FUP-Pv 000019 was included in the data matrix of Fiorelli et al. (2016), which is based on expanded works of Clark (1994), Ortega et al. (2000), Pol (2003), Turner and Sertich (2010), Andrade et al. (2011), Pol et al. (2012, 2014), Leardi et al. (2015a and b), and Martin and De Broin (2016), comprising 440 characters and 113 taxa. Besides the new taxon described here, *L. sigogneaurussellae* was also added to the analysis, increasing the total number of terminals to 115. On the other hand, we excluded highly incomplete taxa (*Coringasuchus*, *Microsuchus*, *Neuquensuchus*, *Pabwehshi*, and *Pehuenchesuchus*) following the protocol used by Fiorelli et al. (2016) and *Chimaerasuchus paradoxus* that, after the revision of its coding, resulted in polytomies among many different clades. Therefore, the data matrix comprises 109 active terminals. The analysis considered all characters as equal weights (Supplementary Information 1–3).

The most up-to-date version of the matrix, published by Cunha et al. (2020), was chosen for the analysis. The updated version of the data matrix used in this analysis can be found in Morphobank (<http://morphobank.org/permalink/?P5622>) and Supplementary Information 2 (NEXUS file) and 3 (TNT file).

The codified characters of all members of Candidodontidae (*C. itapecuruense*, *M. mwakasyungutiensis*, *P. kapilimai*, and *L. sigogneaurussellae*), together with the enigmatic *Chimaerasuchus paradoxus* Wu & Sues, 1996 (Supplementary Information 2 and 3), were revised. This revision was aided by images of the *Pakasuchus* holotype provided by the primary author of that species (Patrick O'Connor) and first-hand study of the *Candidodont* material kept at the Geology Department of the Federal University of Rio de Janeiro. *Malawisuchus mwakasyungutiensis*, *L. sigogneaurussellae*, and *Chimaerasuchus paradoxus* were recodified through direct consulting to the original published works (Wu & Sues, 1996; Gomani, 1997; Ösi, 2014; Pol et al., 2014; Martin & De Broin, 2016).

We also correct cumulative errors in the data matrix. The characters 38, 176, 184, and 262 in the most updated version of the character list (used in this study) are binary, but the

accompanying data matrix has one taxon for each of these characters scored as state 2. These issues only could be identified because we added the characters and character state descriptions for each character in the Nexus file data matrix. Additionally, when uploading this data matrix in Morphobank, the system automatically identified that these four characters had one state with no description. We reviewed the literature in detail to find the source of these problems and provide the reasoning for the changes we made in the Supplementary Information 1.

Ordered characters put in place by Fiorelli et al. (2016) were kept as follows: 1, 6, 10, 23, 37, 43, 44, 45, 49, 65, 67, 69, 71, 73, 77, 79, 86, 90, 91, 96, 97, 105, 116, 126, 140, 142, 143, 149, 182, 193, 197, 228, 279, 356, 357, 364, 368, and 401. However, binary characters were removed from the above ordered list (3, 167, 187, 226, and 339).

The analysis was conducted using TNT 1.6 (Goloboff et al., 2008). A heuristic search was performed due to the high number of taxa in the data matrix, with a randomized taxon addition method to avoid local optima. The first round of analysis used the *New Technology* with all searching methods (Sectorial Search, Ratchet, Drift, and Tree Fusing) activated, the number of random addition sequences was set to 10,000, and the default parameters were kept for the remaining options in this analysis. A second round of analysis used the Traditional Search algorithm and examined the trees from the first round kept in the memory. In this case, the TBR was used as the swapping method and all remaining parameters were kept as default.

The resulting MPTs were stored in memory and submitted to a second round using *Traditional Search* with TBR as a swapping method. A subsequent strict consensus topology was utilized as the working hypothesis. Bremer support and bootstrap values were employed as support indexes for group monophyly.

Institutional Abbreviations—FUP, Faculdade UnB Planaltina, Federal District, Brazil; MAL, Malawi Department of Antiquities, Lilongwe, Malawi.

Anatomical Abbreviations—**a**, angular; **aap**, articular ascending process; **aof**, antorbital fenestrae; **ar**, articular; **ar**, *M. adductor radialis*; **bb**, biceps brachii muscle; **bbt**, *M. biceps branchii tubercle* of insertion; **cbb**, *M. coracobrachialis*; **cbv**, ventralis coracobrachialis brevis muscle; **ccp**, profundus costocoracoideus muscle; **ccss**, superficialis costocoracoideus muscle; **cf**, coracoid foramen; **d**, dentary; **d. inc**, incisive tooth; **dc**, *M. deltoideus clavicularis*; **denti**, denticles; **dpt**, deltopectoral crest; **ds**, distal sulcus; **dv**, dorsal vertebra; **ecrb**, *M. extensor carpi radialis brevis*; **ect**, ectopterygoid; **emf**, external mandibular fenestrae; **ell**, external lateral ligament; **fae**, foramen aerum; **fio**, foramen intemandibular oralis; **fm**, foramen magnum; **fr**, frontal; **fu**, *M. flexor ulnaris*; **glc**, glenoid facet of the coracoid; **h**, humerus; **I–V**, digit numbers; **ip**, lateral process of the radial-humeral articular face; **itf**, infratemporal fenestrae; **j**, jugal; **la.c**, labial cingulum; **li.c**, lingual cingulum; **lk**, longitudinal keel; **m.c**, medial carina; **mc**, metacarpal; **mtr**, medial crest of the triceps; **mx**, maxilla; **n**, nasal; **olp**, olecranon process; **os**, osteoderm; **oto**, otoccipital; **p**, parietal; **pfr**, prefrontal; **ph**, phalanges; **ph.u**, ungual phalanges; **po**, postorbital; **pq**, *M. pronator quadratus*; **poz**, postzygapophysis; **prz**, prezygapophysis; **pt**, pterygoid; **q**, quadrate; **qj**, quadratojugal; **r**, radius; **rf**, radial facet; **rhs**, radial-humeral articular face; **ri**, rib; **rp**, replacement tooth; **sa**, surangular; **sc**, scapula; **sec**, supracoracoideus muscle; **soc**, supraoccipital; **soc.c**, supraoccipital crest; **sp**, splenial; **sq**, squamosal; **ss**, *M. subscapularis*; **stf**, supratemporal fenestrae; **sup**, *M. supinator*; **tbm**, *M. triceps branchii caput mediale*; **u**, ulna; **uf**, ulnar facet; **uhs**, ulnar-humeral articular face; **urhs**, radial-humeral facet of the ulna; **vc**, vertebral centrum.

SYSTEMATIC PALEONTOLOGY

CROCODYLOMORPHA Walker, 1970

MESOEUCROCODYLIA Whetstone & Whybrow, 1983

NOTOSUCHIA Gasparini, 1971 *sensu* Ruiz et al., 2021

CANDIDODONTIDAE Carvalho, Ribeiro, & Ávila, 2004

New Definition—The most inclusive clade containing *Candidodon itapecuruense* Carvalho & Campos 1988 but not *Araripesuchus gomesii* Price 1959, *Peirosaurus tormini* Price 1955, *Sphagesaurus huenei* Price 1950, *Baurusuchus pachecoi* Price 1945, and *Sebecus icaeorhinus* Simpson 1937. This is a maximum clade definition and a converted clade name from Carvalho et al. (2004).

Reference Phylogeny—Phylogenetic hypothesis depicted in this work.

Composition—Based on the reference phylogeny, *Candidodontidae* includes *C. itapecuruense* Carvalho & Campos 1988, *Malawisuchus mwakasyungutiensis* Goman 1997, *Pakasuchus kapilimai* O'Connor et al., 2010, *Lavocatchampsia sigogneaurus-sellae* Martin & Broin, 2016, and *Thilastikosuchus scutorectangularis* (this work).

THILASTIKOSUCHUS SCUTORECTANGULARIS, gen.
et sp. nov.
(Figs. 2–12, and 14)

LSID: urn:lsid:zoobank.org:pub:8D1D5024-1737-4F0B-BC03-C93291934FCB.

Etymology (Genus)—*Thilastikó* (Gr.), meaning ‘mammal,’ in reference to the mammal-like dentition found in members of *Candidodontidae*, and the classic suffix *suchus* (Gr.) meaning ‘crocodile.’

Etymology (Type Species)—*Scutos* (Lt.), meaning ‘armour,’ and *rectangularis* (Lt.) in allusion to the rectangular-shaped dorsal osteoderms.

Holotype—FUP-Pv 000019, a juvenile-adult specimen represented by an articulated skull with partially complete mandibles and dentition, semi-articulated postcranial skeleton, including anterior appendicular elements, and osteoderms.

Type Locality—Campo Azul Municipality, State of Minas Gerais, Brazil; Quiricó Formation, Sanfranciscana Basin; Barremian-Aptian, Early Cretaceous (Lima, 1979; Arai et al., 1995; Carmo et al., 2004).

Diagnosis—Notosuchian of small body size marked by the combination of the following characteristics (autapomorphies are highlighted with an asterisk): (1) triangular-shaped skull in dorsal view (Fig. 4A, B); (2) relatively large rectangular supraoccipital composing the posterior margin of the skull table with a pronounced sagittal torus on the occipital surface* (Fig. 4I, J); (3) a hypertrophied *foramen aereum** (Fig. 4I, J); well-developed heterodonty, with incisiforms and molariforms, the latter always cingulated, often denticulated (Fig. 5); presence of a posterior symphyseal process* (Fig. 4C, D); mediolaterally expanded rectangular dorsal osteoderms with laterally shifted sagittal crests* (Fig. 6C, D, F, G).

DESCRIPTION

General Description

The preserved material belongs to a single individual, as all elements were found in the same portion of rock and there are no duplicate bones, consisting of both cranial and postcranial remains (Figs. 2, 3, 4). The skull is mostly complete, lacking major taphonomic distortions apart from a dorsoventral compression that collapsed the nasals, and with nearly all teeth

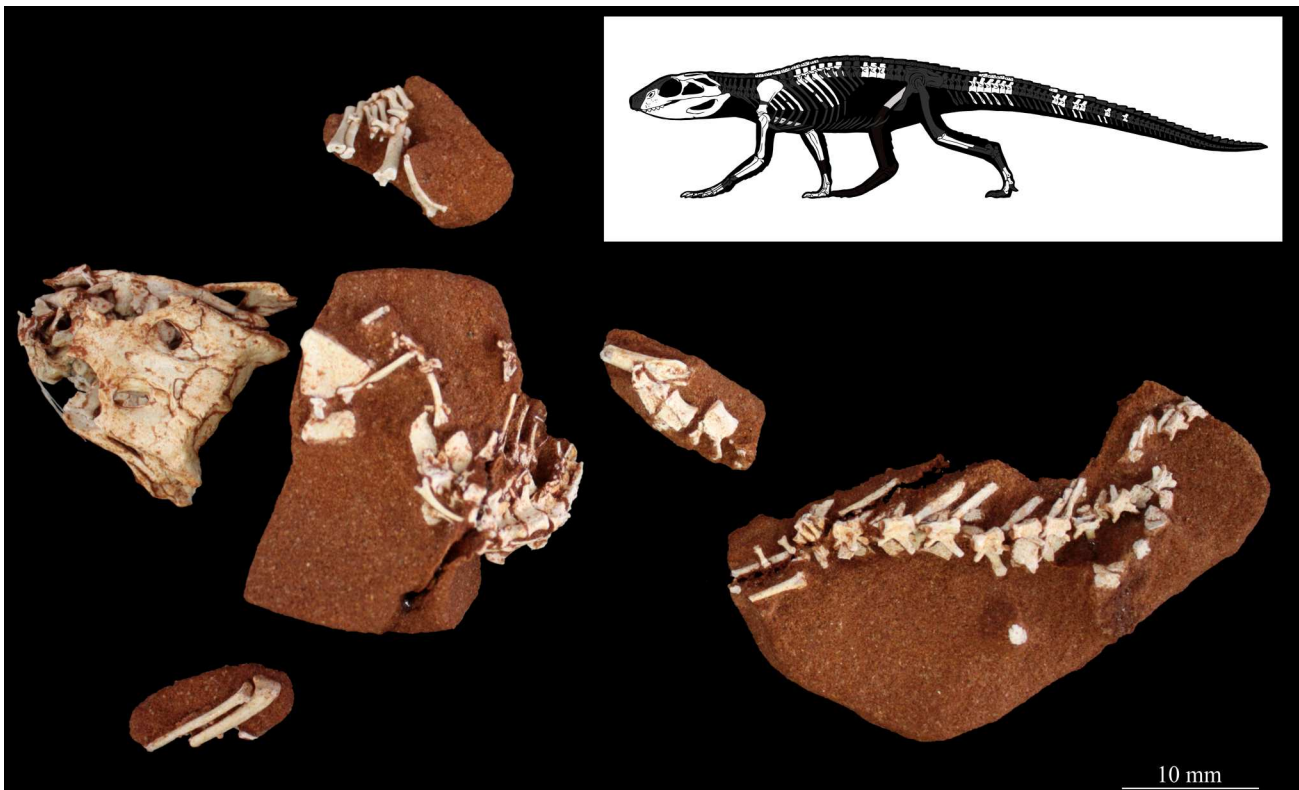


FIGURE 2. Dorsal view of *Thilastikosuchus scutorectangularis*, (FUP-Pv 000019), with skeletal reconstruction in the upper right corner showing the recovered elements (artwork by Felipe Alves Elias). Scale bar equals 25 mm.



FIGURE 3. 3D segmentation of the cranium and mandible of *Thilastikosuchus scuto rectangularis*, (FUP-Pv 000019). **A–D**, skull in **A**, dorsal; **B**, palatal; **C**, left lateral (with mandible); and **D**, right lateral views. **E–G**, mandible in **E**, ventral; **F**, dorsal; and **G**, right lateral views. Scale bar equals 10 mm.

preserved, except by left maxillary and left dentary molariforms. Preserved postcranial elements include the dorsal vertebral series, the right shoulder girdle (scapula and coracoid), the anterior appendicular region, a partially complete caudal series, as well as dorsal and caudal osteoderms (Figs. 2, 9). Bone arrangement and surface textures, with no signs of abrasion, do not support extensive transport.

Cranium

The skull is small and is relatively well-preserved (Figs. 3, 4), measuring 45 mm in rostral-occipital length (ROL), preserving the bone original texture, despite a slight dorsoventral flattening that distorted the original outline of some elements and the presence of a fracture that sectioned it between the orbits and the rostrum, also affecting the mandibles.

Some skull elements have not been preserved, such as the premaxilla, lacrimal, prefrontals, palpebrals, and palatines. Interestingly, it also possesses a series of characteristics consistent with it being a not fully grown individual (as mapped by Griffin et al., 2021; dos Santos et al., 2022, 2024): (1) proportionally large orbits (Figs. 3A, C, D, 4E, F, G, H); (2) cranial sutures not completely fused (Figs. 3A, 4A, B); (3) vertebral neurocentral sutures not fully closed; (4) small supratemporal fenestrae with shallow

fossae (Figs. 3A, 4A, B); (5) incipient sculpturing of dermatocranium (Figs. 3, 4); (6) high pneumatization of cranial bones.

In dorsal and palatal views (Figs. 3B, 4C, D), the cranium gradually changes from a rectangular outline along the skull table posteriorly, to a more transversely narrower, anteriorly tapering rostrum, giving it a triangular-like overall shape. Laterally (Figs. 3C, D, 4E–H), despite a partial collapse of the anterior skull bones, the articulated cranium and mandibles have an elliptical profile, with a straight dorsal margin and an arched ventral one. There is a visible triangular antorbital fenestra between the lacrimal and maxillary bones (Fig. 4F). It is surrounded by a narrow fossa with somewhat rounded vertices, as also seen in forms such as *Candidodon itapecuruense*, *Notosuchus terrestris*, and *Lavocatchampsia sigogneaurussellae* (Carvalho, 1994; Fiorelli & Calvo, 2008; Martin & De Broin, 2016).

The infratemporal fenestrae also display a triangular outline (Fig. 4G, H) and are laterodorsally positioned, being substantially longer than tall. The supratemporal openings, in turn, are elliptical, with the major axis laterally inclined (Fig. 4A, B). The skull roof and temporal regions lack crests but are marked by prominent posterior squamosal processes that project beyond the lateral and occipital margins of the skull. The occipital end is characterized by a relatively thick sagittal torus, with adjacent depressions on the supraoccipital (Figs. 3, 4I–J). The

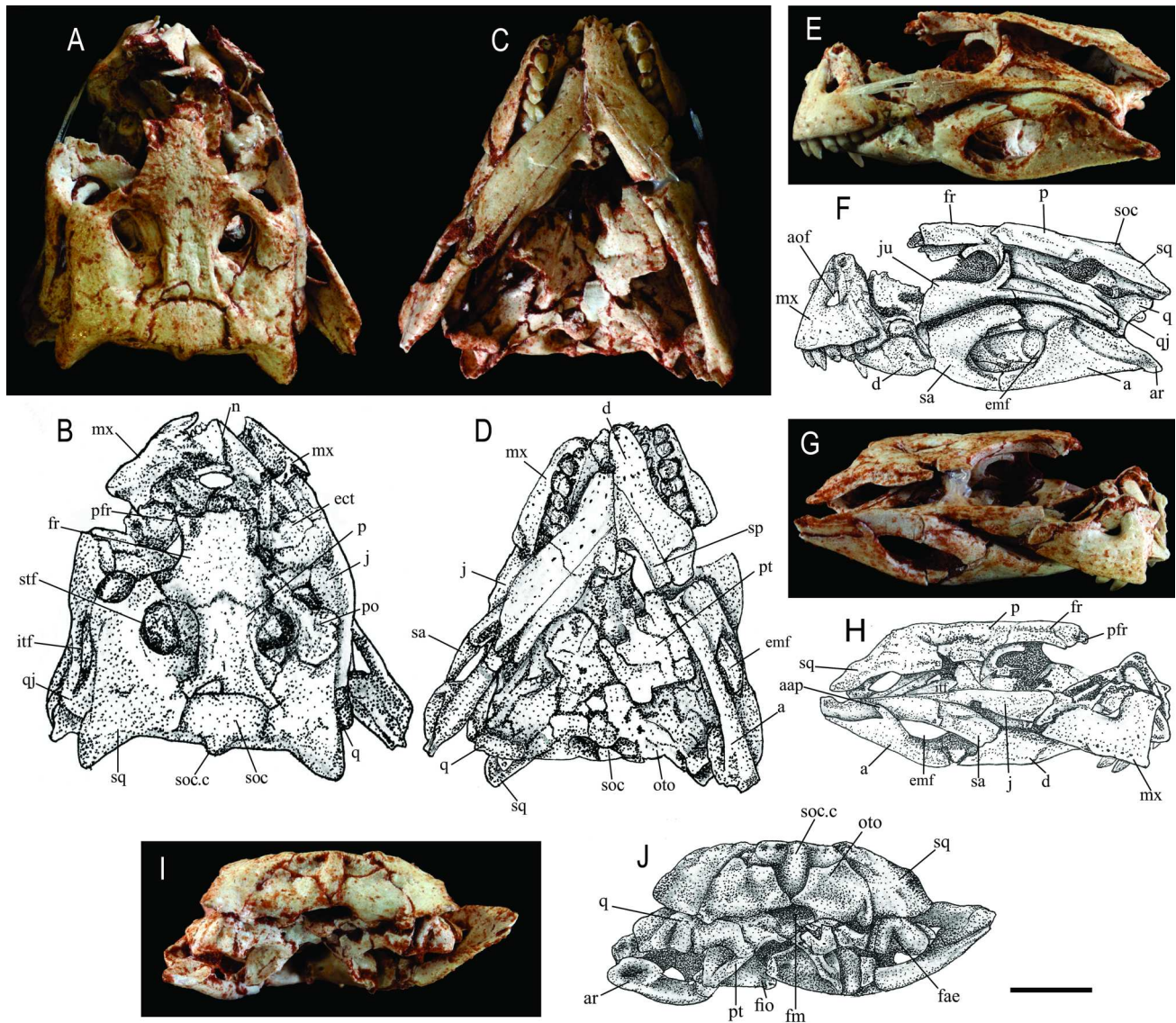


FIGURE 4. Skull of *Thilastikosuchus scutorectangularis*, (FUP-Pv 000019). **A, B**, dorsal view; **C, D**, palatal view; **E, F**, left lateral view; **G, H**, right lateral view; **I, J**, posterior view. **Abbreviations:** a, angular; aap, articular ascending process; aap, articular surface for palpebral; ar, articular; d, dentary; ect, ectopterygoid; emf, external mandibular fenestrae; fr, frontal; fae, foramen aerum; fio, foramen intemandibular oralis; fm, foramen magnum; aof, antorbital fenestrae; itf, infratemporal fenestrae; j, jugal; mx, maxilla; n, nasal; oto, otoccipital; p, parietal; pfr, prefrontal; po, postorbital; pt, pterygoid; q, quadrate; qj, quadratojugal; sa, surangular; soc, supraoccipital; soc.c, supraoccipital crest; sp, splenial; sq, squamosal; stf, supratemporal fenestrae. Scale bar equals 10 mm.

latter does not seem to reach the *foramen magnum*. Despite being broken, it is possible to observe that the pterygoids are developed and posteriorly inclined, forming continuous surfaces that lack fossae, foramina, or fenestrae.

Unfortunately, the choanal openings are damaged, and the level of fragmentation prevents a description of their original morphology (Figs. 3, 4C, D). Still, it is possible to discern a preserved septum between the palatines and pterygoids. The cranial surface is poorly sculptured and mostly smooth, except for small irregularities and minor rugosities (Figs. 3A, 4A, B). The mandibles were fully preserved, including their symphysis and complete right-left rami. Their external mandibular fenestrae (emf) are proportionately large and oval-shaped in lateral view (Figs. 3C, G, 4E–H), located at the posterior ends of the mandibular rami. Both dentary and splenials make up the mandibular symphysis, the latter composing close to 40% of their total length (Figs. 3E, F, 4C, D). Most importantly, the symphysis is also

comparatively longer than in other members of *Candidodontidae*, forming a y-like shape, but lacking a major lateral deflection of the mandibular ramus.

Maxilla—The outer surfaces of the maxillae are partially fragmented and not completely preserved except for the left and right areas surrounding the antorbital fenestrae and the alveolar margin (Figs. 3C, D, 4E–H). The maxillae are semi-articulated, and the dentary is preserved attached to their ventral surfaces, partially obscuring them. Nonetheless, it is possible to observe the suture between counterparts, which are also posteriorly sutured to the palatine, as seen in computed microtomography images. Laterally, the maxillae are characterized by a divergence into an ascending and a ventrolateral process, thus forming the anterior margin of the antorbital fenestrae as they contact the lacrimal posteriorly. No antorbital fossae are present, as opposed to the shallow excavation present in the lacrimal. In transverse section, the

posterior palatine ramus, although highly fragmented, has a sub-triangular and concave shape.

The left maxilla does not have its posterior portion (jugal process) preserved (Fig. 4F). In dorsal view, the external surface of the maxilla forms an almost vertical wall. In its ventral portion, the maxilla is lateromedially thicker and has a complete row of seven teeth. Small circular neurovascular foramina are observed on its lateroventral margin, just above the teeth, these foramina increase in size towards the posterior teeth. These foramina are not equally distributed in both maxillae. In the anterior portion of the maxilla, between the first four teeth, there is an ornamentation consisting of small, spaced circular depressions, which may be observed on both sides (Fig. 4E–H).

Jugal—Although both jugals are present (Figs. 3A, C, D, 4A, B, E–H), the left element is better preserved, allowing for a more detailed description of its morphology. The jugal is a tri-adiate and laterally flattened bone, composed of an anterior ramus that contacts the maxilla, a second dorsomedial ramus that forms part of the postorbital bar, and a posterior ramus that forms the ventral margin of the infratemporal fenestra, fusing to the quadratojugal. The latter two form the anterior and ventral margins of the infratemporal fenestra, respectively. In contrast to the posterior rami, the anterior portion of the jugal is dorsoventrally expanded, forming a triangular and ventrally deflected surface. The jugal is also marked by the presence of an infraorbital crest, which emerges from the posterior ramus and continues anteriorly along the margin of the orbit (Fig. 4G). The process that forms the postorbital bar is cylindrical, slender, and medially inset, ascending and suturing with a similar process of the postorbital. The ventral margin of the element is concave in lateral view, following the shape of the surangular dorsal surface (Fig. 4F). It is in contact with the ectopterygoid in its medioventral region, with the preserved portion elongate and cylindrical. The surface of the jugal does not present any ornamentation.

Nasal—The nasals are partially preserved (Fig. 3A), with only their anterior portions distinguishable. They are paired bones with a clear medial surface for contact between both elements. They are also dorsoventrally flattened and transversely wide near the frontal, with an evident anterior tapering, creating a triangular shape in the dorsal region of the snout. Their preservation state only allows the inference of their contact with the maxillae lateroventrally and the frontal bone posteriorly. Like other skull elements, they do not have an ornamented surface. Due to their fragmented appearance, a degree of nasal pneumatization was revealed, with sediment filling the nasal cavities.

Prefrontal—The fracture that passes through the skull mainly affected the prefrontals, but these still have their posterior portions preserved in contact with the frontal bone, as well as their medial pillars (Fig. 4B, H). The contact with the lacrimals is not preserved. Dorsally, their posterior fragments are wedge-shaped and present a shallow groove near the contact with the frontal bone. Their lateral margins form the anterodorsal rim of the orbits, being slightly elevated in relation to the dorsal surface of the frontal bone. A fracture allowed the observation of the prefrontal pillars, which are not only vertically arranged, but also wide transversely and flattened anteroposteriorly, having a laminar appearance. Near the contact with the nasal bone, the pillars meet in the medial plane, closing the passage of the olfactory bulb.

Frontal—It has a triangular and/or trapezoidal shape in dorsal view (Figs. 3A, 4A, B), considering that its most anterior portion is fragmented. Anteriorly, it narrows as it contacts the nasals and prefrontals. Posteriorly, the frontal enters the supratemporal fossa, and a triple contact including the postorbital and the laterosphenoid can be observed. The suture between the frontal and parietal is V-shaped and transverse (Figs. 3A, 4B). Its dorsal

surface does not have a sagittal crest, which is commonly seen in other notosuchians, being only slightly ornamented with ridges and grooves. In anterior view, the frontal has descending lateral processes (crista cranii), which delimit the olfactory bulbs, as well as a sagittal prominence on the ventral facet, which forms the anteroposterior sulcus of the same (medial crest of the ventral face of the frontal). Anteriorly, it contacts the nasal at the level of the anterior portion, where the absent portions of the orbit would be located. Posteriorly, it is limited by the parietal and postorbital bones, with the posterolateral suture meeting the beginning of the superior temporal opening.

Postorbital—The postorbital is composed of an anteromedial process that contacts the frontal (Figs. 3A, 4A, B), a descending process that forms the orbital bar, and a posterior process that is dorsoventrally flattened, whose projected lateral margin is part of the temporal bar. In dorsal view, the postorbital has the shape of an inverted “L,” not displaying a fossa in its medial margin composing the limits of the supratemporal fenestra. In lateroventral view, it can be observed that both the squamosal and quadratojugal bones contact the postorbital, and the latter can be seen on the ventral face of the temporal bar. The anterior margin of the postorbital is concave and serves as the site for the suture of the posterior palpebrals. In the temporal bar, there are insertion ridges for ear flap muscles. Overall, this element has little ornamentation.

Parietal—It extends from the anterior region of the supratemporal openings to the supraoccipital (Figs. 3A, 4A, B). In dorsal view, it is rectangular and marked by parallel lateral crests that precede its contribution to the supratemporal fossae. Its posterior margin presents a thickening that reaches the squamosal bone, involving the supraoccipital. It does not have sagittal and/or medial crests, being mostly flat dorsally. Besides the frontal bone, the parietal also contacts the laterosphenoid lateroventrally. The parietal does not contribute to the posterior margin of the skull table. This contact can be seen in the supratemporal fossa. The ornamentation is poorly developed.

Supraoccipital—It is located in the posterior cranial roof between the parietal and the squamosals. It has a rectangular shape in dorsal view, while in occipital view, it has a “T” shape due to the presence of a robust vertical bulge (sagittal) that is laterally bordered by small depressions (Fig. 4J). This vertical crest attenuates ventrally, fitting between the exoccipitals but not reaching the margin of the foramen magnum (Fig. 4J). On its occipital margin, there are longitudinal rugosities which, together with the lateral depressions, are evidence of areas for muscular insertion.

Otoccipital—They are broad paired elements located in the occipital region, lateral to the medial bulge of the supraoccipital. They have a wing shape, with a depression in the suture region with the supraoccipital (Figs. 3, 4J). They are vertically and transversely wide and have a small dorsal wedge-shaped process that fits between the supraoccipital and the squamosal. Additionally, the otoccipitals almost entirely make up the foramen magnum, except for its ventral margin, but contribute little to the formation of the occipital condyle itself, which is mainly formed by the basioccipital.

Squamosal—It comprises the upper temporal opening in its posterior portion, and in its mediolateral portion is located between the parietal and its suture with the supraoccipital (Figs. 3, 4). Anteriorly, it contacts the postorbital, the exoccipital posteriorly, and quadratojugal ventrally. Dorsally, it develops a trapezoidal morphology, marked by an acute posterior process that extends beyond the occipital surface. The squamosal is laterally expanded, forming the posterior part of the temporal bar that overlaps the otic recess. This bar is slightly deflected ventrally at its lateral margin. Like other bones in the cranial roof, its ornamentation is poorly developed in the form of irregularities on its surface.

Quadrate—In lateral view, its distal portion is dorsoventrally inclined (Figs. 3D, 4E, F), while ventrally, it presents a medial curvature, where it contacts the bones of the basicranium (basisphenoid and basioccipital) (Fig. 4D, J), as well as the pterygoids. It also contacts dorsally to the squamosal, and ventrolaterally to the quadratojugal (Fig. 4D). The dorsal portion of the quadrate presents a lateral elliptical depression, which composes its otic recess. This is medially deep, with a well-marked otic incisure, and is posterodorsally arranged, where the external auditory meatus (EAM) is inserted, characterized by a large anterior chamber separated from the inner ear cavity itself by a broad septum (otic buttress *sensu* Montefeltro et al., 2016). The latter presents a rounded margin with a slight thickening edge. The distal process of the quadrate develops the lateral and medial condyles, with the lateral one having a larger articulation surface, separated by a ventral groove. In occipital view, the articular process of the quadrate bears a relatively large *foramen aereum* in relation to the total element size (Figs. 3, 4J), which develops from a deep groove that reaches the limit between the condyles (Fig. 4J). Additionally, this portion of the quadrate also presents a posterior acute projection, slightly ventrally projected, which contacts the ventral surface of the posterior process of the squamosal.

It is also important to note a marked ventral concavity present in the quadrate, close to the condyles, which is associated with a shallow groove. Its articular condyles are separated from each other by a shallow notch on its ventral margin. On the dorsal surface, it meets the squamosal and articulates broadly with the quadratojugal rostrally. The quadrate is smooth, as seen in other crocodylians, regardless of their ontogenetic stages.

Ectopterygoid—Located ventrally and partially fragmented, the ectopterygoid in this specimen is an anteroposteriorly elongated element, with an anterior and dorsolaterally inclined process that forms a triple contact with the maxilla and jugal (Figs. 3B, 4). It is excluded from the margin of the alveolus of the most posterior maxillary alveolus, as in *Caipirasuchus* and *Candidodon*, and unlike *Mariliasuchus*, where the ectopterygoid does participate in the lateral margin of the alveolus of the last tooth of the maxilla. Its ventral process is more transversely expanded, composing a long suture with the wings of the pterygoid to form a single solid surface. In palatal view, its anteromedial and anteroposterior margins mark the suborbital fenestra, which appears to have been elliptical with a greater anteroposterior axis. Dorsolaterally, along its contribution to the pterygoid wings, the ectopterygoids become visibly thicker and more robust, increasing the inferred area of insertion of the *M. pterygoideus* muscle group and of the transiliens cartilage.

Pterygoids—The wings of the pterygoids have a triangular shape and are laterally inclined with the apex facing the posterior region (Figs. 3B, 4C, D). They are not thick, being laminar and/or dorsoventrally flattened elements. In palatal view, their posterior margin forms the contact with the basioccipital, which, although fragmented, appears to have had a triangular shape (Fig. 4D). This region is also surrounded by two posterior processes of the pterygoids, which are locally sutured to the quadrates. The pterygoids are also marked by a distinct anteroposterior medial depression, which is exacerbated near the choana. This is located mainly in the pterygoids but also at the ectopterygoid-palatine contact anteriorly. Unfortunately, due to the partial collapse of the skull, the morphology of the choana could not be fully observed, only preserving a putative sagittal septum. Also, due to partial fragmentation, it was possible to distinguish the anterodorsal projection that closes the nasopharyngeal passage.

Basicranial Bones—The components of the basicranium are fragmented due to the dorsoventral compression to which the skull was subjected. However, it was possible to infer a triangular shape for the basioccipital in palatal view, as mentioned previously, which is located among the pterygoids, quadrates, and

basioccipital. The latter is anteroposteriorly thin and is better preserved, forming the occipital condyle in occipital view, and then expanding transversely towards the palatal surface.

Mandible

Dentary—The dentaries are semi-articulated and form a triangle-like shape element in palatal/ventral view (Figs. 3E–G, 4C, D). The right dentary ramus is the best-preserved, with all teeth present, 11 in total. The left portion is fragmented after the 10th alveolus in the medial region. The anterolateral portion of the dentary has a series of deep neurovascular foramina (Figs. 3E–G, 4D, E) that decrease in number posteriorly, becoming more spaced and presenting anteroposteriorly wide grooves until reaching the mid-portion, where ornamentation is absent (Figs. 3E–G, 4D). In lateral view, the dentary presents a ventral curvature or convexity, and is shallow anteriorly (Figs. 3C, G, 4E–H). The symphysis is narrow and has a “y” shape, similar to what occurs in some Sphagesauridae. The symphyseal suture is long and extends from the anterior portion (anterior tip of the dentary) to the level of the distal border of the eighth tooth, where the mandibular ramus deflects laterally from the sagittal plane (Figs. 3E, F, 4D).

Splenial—The splenial symphyseal contribution has a triangular shape in ventral view, followed by lateromedially compressed posterior process that medially closes the Meckelian canal. It is robust and convex in its medial portion, giving the posterior end of the mandible a slightly sigmoid shape in occlusal view (Figs. 3, 4D). It is well preserved in the right mandibular ramus and fragmentary in the left one at the mid-posterior portion. In ventral view, at the anterior portion, the splenial contacts the dentary, extending to the symphyseal region and participating in an extensive portion of the mandibular symphysis, up to 40%. In posteroventral view, the splenials form the anterior edge of the mandibular adductor fossa. As previously mentioned, a peg-like process is present at the posterior symphyseal margin of the splenial, anterior to the foramen intermandibularis oralis (fio), which is a single opening on both sides. The dorsal edge of the splenials in the mid-posterior region delimits the lingual margin of alveoli. Ventrally, the splenials are mostly flat, but become slightly concave at the tip of the symphysis. Adjacent to the symphyseal process is the foramen intermandibularis oralis, which has an oval shape and is well-developed (Figs. 3E–G, 4). In dorsal view, the symphysis displays a canal-like surface.

Angular—It is a laterally compressed and arched element composing the ventral margin of the external mandibular fenestra and thus the posteroventral portion of the mandibles. It contacts the dentary anteriorly (being overlapped by it laterally), the splenials anteromedially, marking the anterior margins of the mandibular adductor fossa, the surangular posterodorsally and the articular posteriorly, sending a ventral support process where it rests upon. In lateral view, the angular is ventrally convex, with a relatively tall posterior laminar process and a tubular, tapering, anterior one. The former is marked by an ascending hook-like projection that almost reaches the surangular dorsal edge, a feature also seen in *Pakasuchus* and *Malawisuchus* but not to the same extent (Gomani, 1997; O’Connor et al., 2010; Ósi, 2014). Bound by lateral and medial walls, it also bears a longitudinal trough/sulcus with internal neurovascular foramina that extends anteriorly into the Meckelian canal. Medially, along the adductor fossa, the angular lacks a prominent bulged margin, a site for the attachment of *M. adductor mandibulae posterior* (mAMP), being mostly a low relief and with rectilinear wall. This could be due to its ontogenetic stage, but homologous structures could not be seen in other candidodontids for comparisons.

Surangular—The surangular is elongated and slightly dorsally convex in lateral view. It is located in the posterodorsal portion of the mandibular ramus, forming most of the dorsal border of the external mandibular fenestra, where it presents its highest convexity (Figs. 3C, E–G, 4E–H). It is also gently curved in its posterior region, where it contacts the articular bone. In lateral view, in the posterodorsal region, its suture with the angular is visible (Fig. 4F, H). It has a smooth surface devoid of ornamentation and anteriorly consists of a single lamina that overlaps the dentary but does not reach the level of the posterior end of the tooth alveoli. The anterior process of the surangular is not forked but has a rounded anterior end.

Articular—The articular is comprised of a small and dorsoventrally flat element located at the posterior end of the mandibular ramus, resting on a posterior depression of the angular; it is a robust and horizontal bone that is also connected to the surangular laterally (forming a large suture) (Fig. 4). Only the element on the left dentary ramus was preserved. In mediadorsal view, it has a prominent crest that extends from the articular to the angular. The glenoid region projects medially and has a subcircular shape, and is limited posteriorly by a low-relief transverse crest, followed by the retroarticular process. The retroarticular process itself is circular and transversely expanded, with a lateral concave surface and a shallow depression mediadorsally. The medial flanges project posteroventrally. In dorsal view, two pairs of foramina can be observed in the anterior region of the retroarticular process.

Maxillary Teeth—This series lacks developed caniniforms and consists only of subconical (incisiform) and molariform teeth (Fig. 5A). As counterparts to the dentary series, posterior molariforms are multicuspoid, oval in occlusal view, and are obliquely oriented relative to the tooth row, features shared with

Yacarerani boliviensis, *Notosuchus terrestris*, *Adamantinasuchus navae*, *Sphagesaurus huenei*, and *Lavocatchampsia sigogneaurussellae*.

The first tooth in both maxillae is conical and vertically implanted, with a constricted root that is smaller than the ones in the remaining teeth (Figs. 3B, 5A). The second tooth has a subconical morphology, with convex mesial and distal portions of the crown. In the second tooth of the left maxilla, a preserved replacement tooth can be observed (Fig. 5D). The third element is an incipient molariform (m1). The apex of its crown consists of two cusps, the mesial one being higher than the distal one (Fig. 5A), even though the apex of the mesial cusp of the right jaw is worn (damaged). On the mesiolabial and distolabial portions, there is a cingulum with two small accessory cusps on its edge. In lingual view, an accessory cusp is observed at the base of the crown, but the cingulum is absent.

The fourth tooth, m2, is more robust than the previous three teeth and has a high central cusp and two smaller ones (mesial and distal), with the apex of both cusps preserved. Between the crown and the root there is a well-marked cingulum. This feature is also observed in the other maxillary molariform teeth. At the base of the crown, a cingulum extends along its entire perimeter. The labial region has two accessory cusps and, on the lingual portion of the cingulum, only a single cusp is found.

The fifth tooth (m3) has a more robust crown than the fourth one (m2), which is similarly made up of a high central cusp and two smaller ones (mesial and distal). A cingulum is also present, extending from the labial to the lingual portion, extending the entire length of the crown. The cingulum has two accessory cusps on its edge (both on the lingual and labial portions). At the junction of the crown and root, there is a constriction, as seen with previously described molariforms.

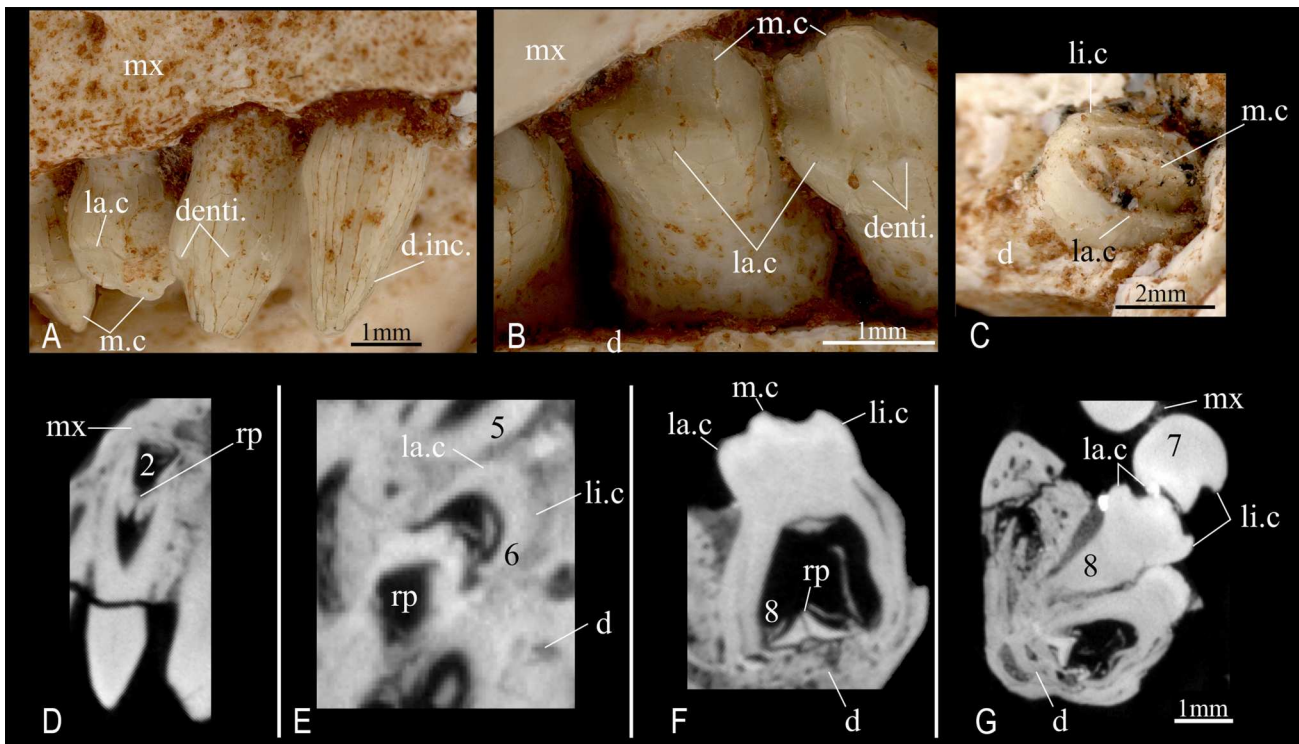


FIGURE 5. Teeth of *Thilastikosuchus scutorectangularis*, (FUP-Pv 000019). **A**, left maxillary teeth in labial view; **B**, **C**, dentary teeth in **B**, labial view and **C**, occlusal view of the last right dentary molar. **D–G**, transverse section of microtomography of maxillary and dentary teeth in **D**, second maxillary tooth; **E**, sixth dentary tooth with replacement tooth; **F**, eighth dentary tooth; and **G**, 11th maxillary tooth and eighth dentary tooth. **Abbreviations**: **d**, dentary; **denti.**, denticles; **d. inc.**, incisive tooth; **la.c.**, labial cingulum; **li.c.**, lingual cingulum; **m.c.**, medial carina; **mx**, maxilla; **rp**, replacement tooth (numbers indicate tooth position). Scale bar equals 1 mm.

The sixth tooth (m4) has a shorter, stouter, and wider crown than the previous molariform teeth. The crown has three cusps, like the molariform m3. Between the crown and root there is a constriction, as in the previous molariforms. Due to the broad surface of the tooth, the cingulum is concave, and there are two accessory cusps on both labial and lingual edges.

The seventh tooth (m5) is preserved only on the right maxilla. Its crown and root are much more robust than the other preserved maxillary teeth (Fig. 5G). The cingulum is well-marked, giving it a concave aspect. The crown has three cusps: a higher central cusp, which seems to be slightly worn, and two smaller ones on the mesial and distal portions. On the labial portion of the cingulum, it is possible to observe accessory cusps (denticles), as well as on the lingual portion (Fig. 5A).

Dentary Teeth—These are mostly multicuspid and may be divided into incisiforms and molariforms. In total, the right dentary ramus preserves 11 teeth, while the left side displays only nine teeth. Caniniforms are not present (Figs. 3F, 5A–C). The dental series is marked by a high degree of heterodonty, varying in form from small conic/subconic incisors to posterior, more robust denticulated molariforms (Fig. 5B, C). Through CT imagery, it was possible to establish that all root lengths exceeded crown heights (Fig. 5F). Except for the very first molariform tooth (first four in the series), all the following are marked by a cingulum with numerous accessory cusps/denticles surrounding the crown base (Fig. 5B). Both cingulum shape and cuspid number vary along the series, and, despite anterior teeth not being cingulated, a slight constriction is observed at the root-crown interface on all elements.

The first dentary teeth (d1) are small, conical and unicuspid, also being substantially procumbent. The crown apex is roughly oval in cross section. Both d2 and d3 follow a conical pattern similar to the first one, though their crowns are slightly higher than those of the first tooth, presenting an oval apex and showing no evidence of a cingulum. Further along the series, the fourth teeth (the last incisor) in both dentaries have one cusp and subconical shape. Its crown is slightly smaller than the second tooth and, like the two teeth described earlier, has no evidence of a cingulum. Its crown apex in occlusal view is oval and projects lingually, sloping gently towards the posterior portion of the dentary.

The d5 and d6 are bicuspid molariforms with a higher mesiolabial cusp and a smaller linguo-distal one, both with a subconical shape. Their crowns are mesiodistally longer than the third tooth, with an oval apex in occlusal view and a more robust base than the previous teeth. There is no evidence of a cingulum on d5, as in the four incisors previously described, but one is present on the sixth tooth. They are mostly subconical, and the base of their crown is larger than the previous teeth. The root is wider than the crown compared with the first three teeth.

Similarly, the d6 is also a subconical and bicuspid molariform. It has a higher cusp on the mesial portion and a smaller one on the distal portion. The crown is much more robust than the two previously described molariform teeth. At the base of the crown, there is a cingulum with further developed accessory cusps, two on the labial side and three on the lingual side. A replacement tooth can be observed in the right d6 using microtomography (Fig. 5).

The seventh tooth is tricuspid, with a higher central cusp and two smaller labial and lingual ones. The crown is wider and more robust, but comparatively shorter. Its cingulum extends along the labial and lingual margins of the crown. On its edge, there are accessory cusps (or denticles), three on the labial side and three on the lingual side (Figs. 3, 5F).

Multicuspid crowns emerge at the eighth tooth onward, marked by a high central cusp and smaller adjacent ones. The crown is shorter in relation to anterior molariforms. The 10th tooth is the most robust molariform tooth, centrally characterized by a crest-shaped cusp. As expected, it also has a cingulum

that surrounds the entire lingual and labial portion, but unlike the others, it does not have accessory cusps surrounding this structure (Fig. 5C).

Replacement Teeth—There are at least nine replacement teeth observed in the cross-sectional computed tomography imagery. These are visible in the maxilla and dentary (Fig. 5D–G). Their degree of development does not present any defined pattern and they are located in the following dental positions: second and fifth teeth of the left maxilla (Fig. 5) and third, fifth, and sixth teeth of the right maxilla (Fig. 5E); first, sixth, and eighth teeth of the left dentary (Fig. 5F), and fourth tooth of the right dentary. The visible portions of replacement teeth consist only of crowns (Fig. 5D, E, F), which have the same shape as the functional teeth (the teeth in the anterior region of both dentary and maxilla have high crowns, and the posterior maxillary and dentary teeth have low crowns), but are sharper, probably due to lack of wear.

Postcranial Skeleton

Dorsal Vertebrae—The preserved elements are comprised of a sequence of seven articulated vertebrae from the anterior and middle portions of the dorsal series, as evidenced by their increasing size towards more posterior preserved elements and by the presence of ribs still attached to some vertebrae (Fig. 6A, B). Only small portions of the vertebral center and transverse processes of some preserved vertebrae are missing.

The middle portion of the preserved series, dv3, dv4, and dv5, has the best-preserved centrum. The vertebral centra are spoon-shaped and slightly amphicoelous/amphiplatyan, with anteroposteriorly concave lateral and ventral faces. Fragmented centra show that the spongy bone tissue is not well-developed. Poorly developed neurocentral sutures are visible in dorsal vertebrae, unlike in the caudal ones, where neurocentral sutures are fully fused and non-visible. The neural arches occupy the entire dorsal surface of the centrum in lateral view.

The neural canals are not easily observable in all preserved dorsal vertebrae due to the position of the material embedded in the rock matrix, except for those that have part of the neural arch fragmented, where the neural canal is visible. The neural canal is slightly wider than tall. It is relatively large, occupying nearly the entire dorsal portion of the centrum so that the walls of the neural arch are transversally thin.

The parapophyses, diapophyses, prezygapophyses, and postzygapophyses are preserved in most of the recovered sequence of the dorsal vertebrae. However, they are not fully visible (Fig. 6H) because they remain articulated to each other. The parapophyses are shorter than the diapophyses, tilting slightly forward and projecting horizontally to the sides. In transverse section, the parapophyses of the preserved anterior vertebrae are elliptical, reinforced ventrally by a centro-parapophyseal lamina/protuberance. This condition changes as one moves towards more posterior vertebrae, where the parapophyses become more dorsoventrally flattened, and the centro-parapophyseal lamina/protuberance disappears.

The diapophysis is longer than the parapophysis and projects upward and backward in more posterior dorsal vertebrae, so that its distal joint is positioned slightly above the parapophysis. Like the parapophysis, the diapophysis presents a centrodiaepophyseal lamina/protuberance. In transverse section, it is elliptical, with the longer axis directed anteroposteriorly. In the more preserved posterior thoracic vertebrae, the parapophysis and the diapophysis have a diapophyseal-parapophyseal lamina.

The prezygapophysis appears to be a small protuberance projecting from the anteroposterior margin of the parapophysis. The postzygapophysis is a protuberance that projects more laterally than posteriorly from the base of the neural spine. The neural spine is a flat, laterally compressed, and anteroposteriorly long

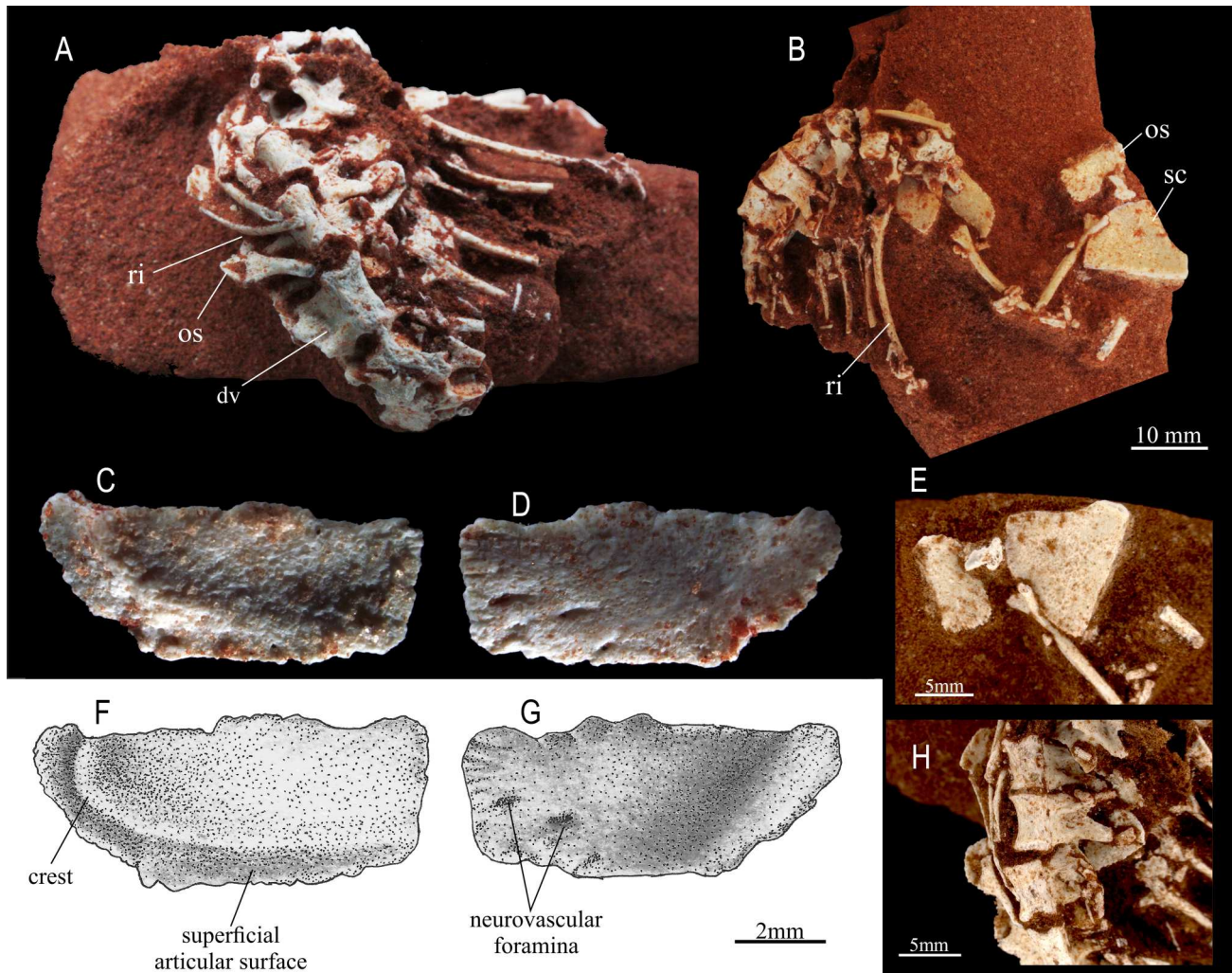


FIGURE 6. Axial skeleton of *Thilastikosuchus scuto rectangularis*, (FUP-Pv 000019). **A, B**, anterior dorsal vertebrae, ribs, and some osteoderms; **C, F**, dorsal view of a dermal plate from the mid-dorsal region; **D, G**, ventral view of the same dermal plate; **E**, dorsal view of scapula; and **H**, detail of mid-dorsal vertebrae in left lateral view. **Abbreviations:** **dv**, dorsal vertebra; **os**, osteoderms; **ri**, rib; **sc**, scapula. Scale bars equal 10 mm in **A, B**; 2 mm in **C, D, F, G**; 5 mm in **E, H**.

structure. As far as can be observed, it is not supported by any lamina.

Caudal Vertebrae—There are 13 articulated and semi-articulated vertebrae from the mid-posterior caudal portion preserved in FUP-Pv 000019 (Fig. 7A). Their position in caudal series is inferred due to their general morphology and position to the remaining bones. These are generally well preserved, although some do not have neural spines. The vertebral centra of some vertebrae are fragmented, whereas the haemal arches are preserved and often in their original position. The vertebral centra are slightly amphicoelous and completely fused to the neural arch in the most posterior caudal vertebrae unlike the preserved dorsal vertebrae where the neurocentral suture is not completely closed, following a similar pattern to modern crocodylians (Brochu, 1996).

In general, the vertebral centra in the most anterior caudal vertebrae have a spool-like shape (Fig. 7B, C), while in the more posterior ones, they are more rounded. The articulations are circular in the preserved anterior caudal vertebrae, and their ventral face is laterally flat and anteroposteriorly concave. In some caudal vertebrae, the ventral face has a subtle pronounced crest in the posterior portion. In ventral view, the ventral face narrows in the central portion of the centrum and, in most

posterior caudal vertebrae, the ventral face is concave and presents a smooth and transversely rounded profile. The lateral faces are concave anteroposteriorly, with a shallow and rounded depression just below the transverse process in the more anterior caudal vertebrae, being dorsoventrally flattened and elongated in the posterior caudal vertebrae.

The transverse process is located nearly at the base of the neural arch, predominantly occupying the upper edge of the vertebral body. They are well-developed and projected backwards at an angle of approximately 45°. They also project slightly upwards and emerge from the dorsal limit of the vertebral body. The transverse processes are flattened dorsoventrally, with a laminar profile in lateral view. In the ventral and posterior portions, a lamina is observed, which is attached to the posterior ventral margin and extends to the posterior portion of the vertebral body. These features are present only in the first five preserved caudal vertebrae. In dorsal view, the transverse process has an incipient lamina/protrusion that connects to the neural spine, bordering the dorsal portion.

The neural arch is relatively low and occupies almost the entire dorsal portion of the vertebral body, being anteroposteriorly long. The prezygapophyses are slender, relatively short (Fig. 7B), and extend slightly beyond the anterior articulation margin of the

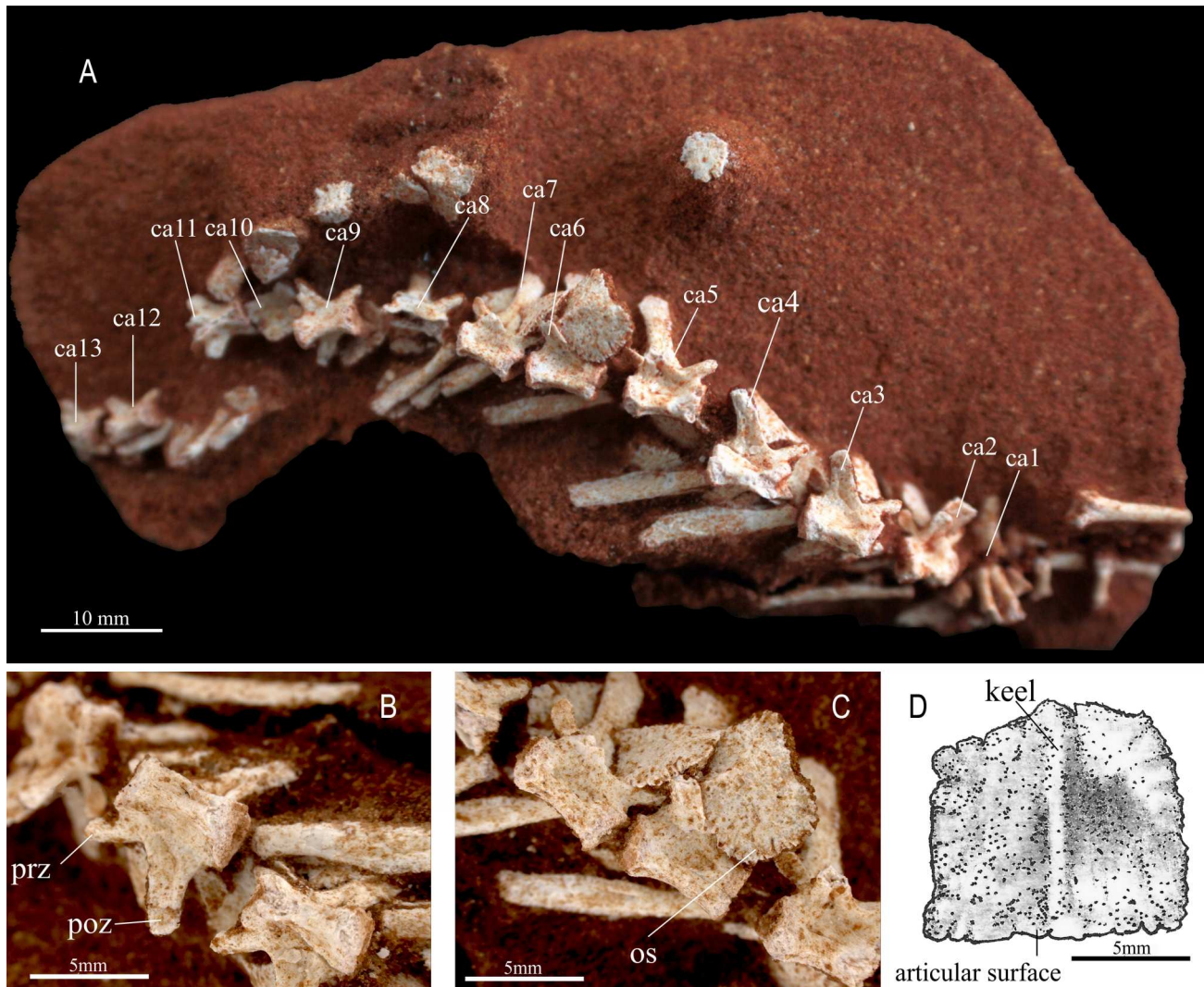


FIGURE 7. Caudal vertebrae of *Thilastikosuchus scutorectangularis*, (FUP-Pv 000019). **A**, articulated sequence of anterior caudal vertebrae; **B**, ventral view of a caudal vertebra; **C**, caudal vertebra and respective dermal plate; and **D**, illustration of the caudal dermal plate in dorsal view. **Abbreviations:** **ca**, caudal centrum; **os**, osteoderm; **poz**, postzygapophysis; **prz**, prezygapophysis. Scale bars equal 10 mm in **A**; 5 mm in **B**, **C**; and 2 mm in **D**.

centrum, being also slightly projected laterally. Apparently, the prezygapophyses are not supported by any structure, except for a robust spinoprezygapophyseal lamina. The articular facets are elliptical, flat, and face inward in the first preserved caudal vertebrae, and face upwards in the posterior caudal vertebrae.

The postzygapophyses comprise a simple projection that originates at the base of the neural spine and is not supported by any lamina. The articular facets are elliptical, flat, facing outward in anterior caudal vertebrae and facing downward in posterior caudal vertebrae.

The neural spine is broken and not visible in the four most anterior caudal vertebrae, except for a fragment in Ca2. The neural spine is laterally flattened, slightly inclined backwards, with its base wider anteroposteriorly due to the presence of the previously mentioned spinoprezygapophyseal and the postspinal laminae. The distal end of the neural spine is rounded and slightly more expanded anteroposteriorly than in its middle portion.

Eleven haemal arches are preserved and, although some of them are not exactly articulated to their respective vertebral centra, they are close to their original position. Considering the morphology of the vertebral centra and the presence of

ventrolateral crests on the posterior portion of them, apparently these haemal arches articulated at the ventroposterior edge of each centrum. Although there is some uncertainty about the original position of the haemal arches in the tail, all of them are inclined backwards. The haemal arches are laterally flattened, both in the articular and distal rami. The haemal arches associated with more anterior caudal vertebrae are longer, with relatively short articular processes, the distal process being four times larger than the articular ones. The haemal canal is relatively narrow and opened dorsally. However, it is uncertain whether the narrowness of the haemal canal is due to a lateral flattening caused by the fossilization process. Apparently, the deformation effect does not apply for two reasons: first, the preserved caudal vertebrae in the same position have no signs of deformation, and the ventral face of the caudal vertebrae is also narrow, indicating that the haemal arch joints would not be too far apart laterally. The articulation with the centrum is not well-developed, and the distal portion of the haemal arch has a nearly square profile. The haemal arches decrease in size towards the posterior portion of the tail, being only half the size of the haemal arches associated with anterior caudals.

Ribs—There are 14 preserved dorsal ribs, seven on each side (right and left), two of them disarticulated. The anterior ribs on both sides are better preserved, and the posterior ones have only preserved portions of the capitulum and the tuberculum. The capitulum is more developed (longer) than the tuberculum in all ribs. Generally, the capitulum originates from the main axis of the rib. The tuberculum, instead, is a divergent axis. There is a lamina that develops between both rami. This region is depressed in lateral and medial views, showing a concavity. Considering the preserved ribs, the anterior ones are larger and more arched, while the posterior ribs are straighter. In cross section, the anterior ribs are elliptical, and the posterior ones are more circular. On the anterior and posterior margins of the most anterior ribs, a well-developed crest is observed along the diaphysis. On the preserved anterior ribs in lateral view, there is a slightly developed crest that emerges from the junction between the capitulum and the tuberculum and occupies the entire lateral surface of the diaphysis.

Coracoid—The left coracoid is complete and well preserved, measuring 16 millimeters in length (Fig. 8). The proximal end is expanded and has a roughly rectangular profile. At the region where the supracoracoideus muscles were inserted, the profile of the bone in lateral view is rounded. The glenoid area is the thickest portion of the proximal end.

The profile of the scapular articular surface is rounded (Fig. 8A, C), differing from the “I” and sub-rectangular shape of most notosuchians. In general, the expansion of the proximal joint is less pronounced than in other notosuchians, such as *Simosuchus* and *Yacarerani*, for example. Around the entire glenoid joint, a well-defined lip-like contour is observed. The coracoid foramen is located near the proximal margin, and has a circular shape, being located at the boundary of the glenoid joint region with the scapula.

The diaphysis is flattened, being thinner in the distal portion. Just posterior to the glenoid articulation, there is a poorly developed posterior glenoid oblique crest that extends along the diaphysis of the coracoid. It has a depression for the insertion of the *biceps brachii* (bb) and the *supracoracoideus* (scc) (Fig. 8B) but does not have a depression for the insertion of the scapulo-external ligament.

The distal portion of the coracoid is twisted in relation to the proximal region, forming a 90° angle. The posterior region is more expanded than the anterior end, and is also more flattened

and expanded dorsoventrally, with the ventral expansion being more developed than the dorsal one. However, it does not have the same development as in *Simosuchus*. In lateral view, this posterior region has a wide and smooth depression, which represents the muscular insertion of the *M. coracoideus profundus* (ccp), *M. superficialis costocoracoideus* (ccss), and *M. ventralis brevis coracobrachialis* (cbbvs) (Fig. 8D). In medial view, the diaphysis does not present any depression.

Scapula—The scapula is broken, lacking the anteroventral region, being comprised of most the scapular blade (Fig. 6E). Only the posterodorsal and middle portions of the diaphysis are preserved. As the specimen was prepared articulated with other bones, only its medial region can be observed. The diaphysis cross section is lateromedially expanded, with a thinner ventroposterior margin. The middle portion of the diaphysis, which separates the anterior and posterior portions, is more constricted. The posterodorsal (acromial area?) is mildly developed.

Humerus—Only the right humerus is partially preserved (Fig. 9A). The dorsal portion of the proximal epiphysis is fragmented, as well as the distal condylar portions, precluding a more detailed description of the morphology of these regions. The humerus is characterized by being a thin element, with an elongated and mostly straight diaphysis, with only a gentle posterior curvature, as well as an anteroposteriorly flattened proximal epiphysis, but transversely wide, with a large triangular depression in its anterior portion (Fig. 9D, E, F, G, H, I). The cross section of the diaphysis is nearly circular.

The distal metaphysis is broken nearly at the portion of the development of the condyles, but part of a vertical intercondylar groove, separating the lateral and medial ridges that would lead to the condyles, is preserved. The proximal epiphysis is marked on its lateral margin by the deltopectoral crest, which consists of a prominent thickening with a medially curved apex. Unlike some Late Cretaceous notosuchians, in *Thilastikosuchus* (as well as in *Araripesuchus tsangatsangana*), the distal portion of the deltopectoral crest does not project ventrally and, therefore, does not fully reach the humeral diaphysis (Pol et al., 2012; Turner, 2006). The aforementioned large anterior depression is interpreted here as the area of insertion of the *M. coracobrachialis brevis* (Fig. 9E) (cbb *sensu* Sertich & Groenke, 2010), which is limited laterally by the deltopectoral crest and medially by the concave margin and the projection of the medial humeral process. Although tomographic images do

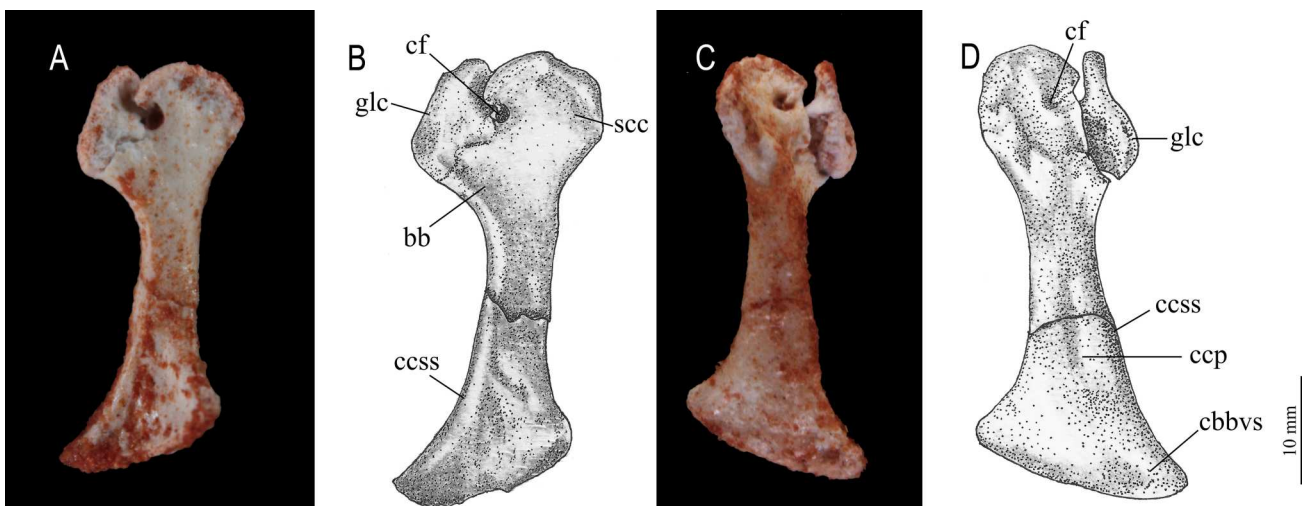


FIGURE 8. *Thilastikosuchus scutrorectangularis*, (FUP-Pv 000019). Left coracoid in posterior (A and B) and lateral (C and D) views. **Abbreviations:** bb, biceps brachii muscle; cbbvs, ventralis coracobrachialis brevis muscle; ccp, profundus costocoracoideus muscle; ccss, superficialis costocoracoideus muscle; cf, coracoid foramen; glc, glenoid facet of the coracoid; scc, supracoracoideus muscle. Scale bar equals 5 mm.

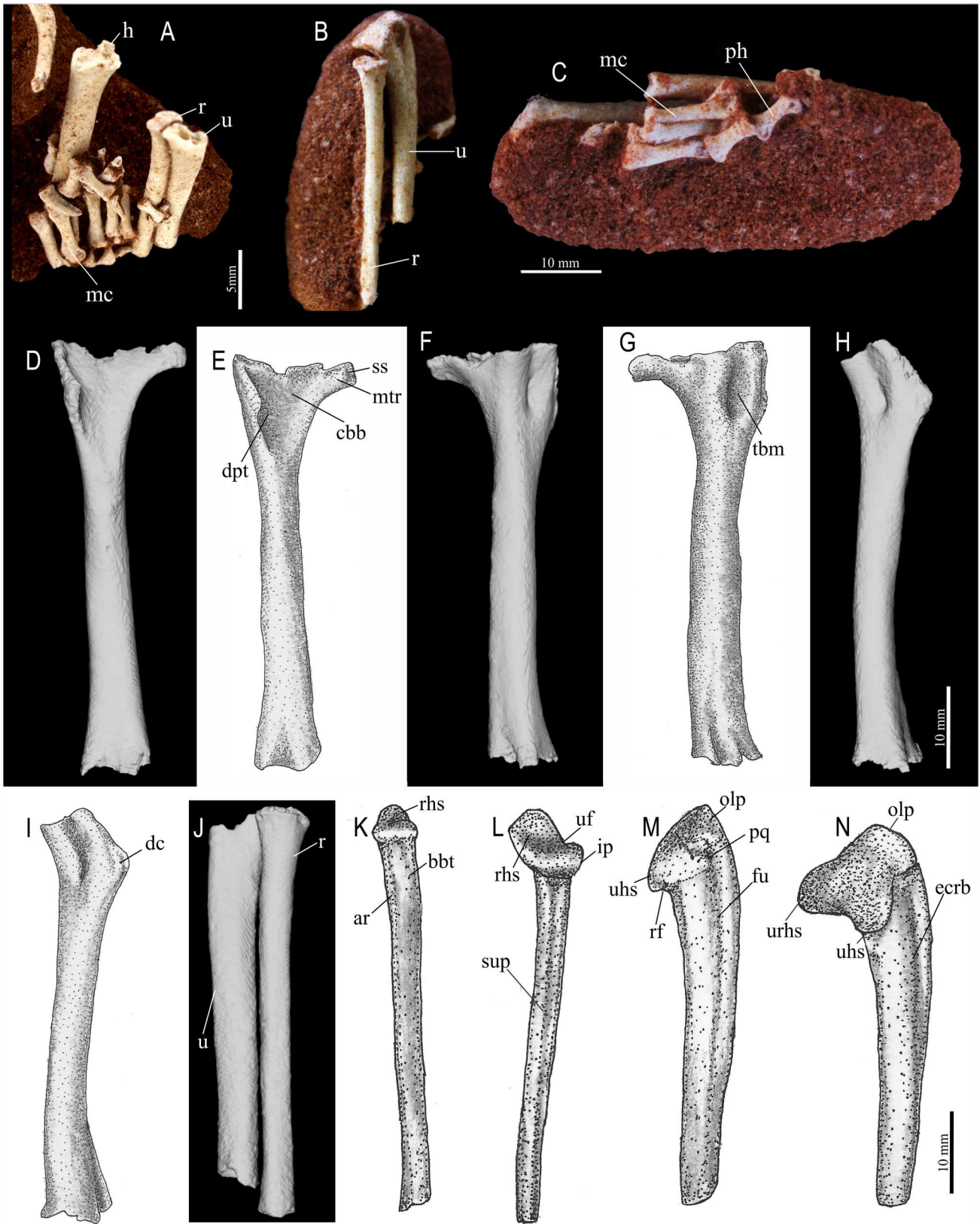


FIGURE 9. 3D segmentation and drawings of the bones of the anterior appendicular portion of *Thilastikosuchus scutorectangularis*, (FUP-Pv 000019). **A**, articulated right hand and arm in dorsal view; **B**, **C**, articulated left hand and partial arm; **D**, **E**, anterior view of the right humerus; **F**, **G**, posterior view of the right humerus; **H**, **I**, lateral view of the right humerus; **J**, right radius and ulna; **K**, **L**, left radius in lateral view; **M**, **N**, left ulna in lateral view. **Abbreviations:** ar, *M. aductor radialis*; bbt, *M. biceps branchii tubercle* of insertion; cbb, *M. coracobrachialis*; dc, *M. deltoideus clavicularis*; dpt, deltopectoral crest; ecrb, *M. extensor carpi radialis brevis*; fu, *M. flexor ulnaris*; h, humerus; ip, lateral process of the radial-humeral articular face; mc, metacarpal; mtr, medial crest of the triceps; olp, olecranon process; ph, phalanges; pq, origin of the *M. pronator quadratus*; r, radius; rf, radial facet; rhs, radial-humeral articular face; sup, *M. supinator*; ss, *M. subscapularis*; tbm, *M. triceps branchii caput mediale*; u, ulna; uf, ulnar facet; uhs, ulnar-humeral articular face; urhs, radial-humeral facet of the ulna. Scale bars equal 5 mm in **A–C** and 10 mm in **D–N**.

not allow the visualization of muscle insertion scars, the position of the *M. pectoralis* and *M. supracoracoideus* groups was inferred at the anterior apex of the deltopectoral crest, which is the thickest region of the crest. A substantial medial extension of the preserved humeral process of the proximal epiphysis is preserved, which, consequently, gives to the medial margin a curved contour. This forms the anterior region for the origin of the *M. triceps brachii caput mediale*, which extends along the diaphysis (Fig. 9D, F, I).

The medial humeral process has a superficial irregularity that can be interpreted as the insertion area for the *M. subscapularis* (Fig. 9E). In posterior view, the proximal epiphysis presents a prominent vertical crest that separates its medial portion from the region that limits the deltopectoral crest. Between these portions, a marked depression develops, which potentially marks the boundaries between the medial head for the *M. triceps brachii* and its lateral head (Fig. 9D, E, F, G, H, I). Dorsally, the insertion region for the *M. scapulohumeralis* was not completely preserved. The diaphysis, in its middle region, has a subcircular/subtriangular cross section and, together with the metaphysis, presents a relatively smooth periosteal surface.

Radius—Both right and left radii are preserved. They partially articulated with the ulna (Fig. 9A, B). The left element is better preserved, including its proximal articular end, but not the distal one. The right radius, even though incomplete, is 2.4 mm in diameter, marked by a straight, slender, and elongated diaphysis, with the proximal epiphysis with a rectangular contour and rounded sides.

The medial portion of the diaphysis has a gentle anteromedial inclination. The articular surface has a slight concavity that articulates with the condyles of the humerus. On the lateral margin, a slight expansion is observed, deflecting ventrally to the proximal facet of the ulna. Anterior to the proximal articular surface, a well-marked scar/groove can be identified that extends along the diaphysis to the distal region, where the lateral margins of the *M. supinator* are located (Fig. 9J, K, L).

Ulna—Both left and right ulnae are preserved, and similarly to the radius, the left one is in better condition, with the proximal articulation intact (Fig. 9A, B). The ulna is anteroposteriorly shorter than the radius, measuring approximately 1.9 mm in diameter. The diaphysis is mediolaterally constricted compared with its proximal end. In proximal view, the ulnar articular surface is observed, which has a subtriangular shape, composed of a bilobed articular surface for the radius and humeral condyles.

At the distal end, ventrally to the olecranon process, it is possible to observe the insertion area of *M. triceps brevis*. In a lateral view, there is also a longitudinal groove in this surface, as well as a rectangular-shaped olecranon process displaced from the main axis of the diaphysis, interpreted here as the limit between the dorsal *M. extensor carpi radialis brevis* and the ventral *M. flexor ulnaris* (Fig. 9M, N) (Meers, 2003; Sertich & Groenke, 2010). In anterior view, it is possible to distinguish a longitudinal crest that extends along the diaphysis, also present in the ulna of other taxa (e.g., *Simosuchus clarki* Sertich & Groenke, 2010; *Yacarerani* Leardi et al., 2015b). Below the proximal articulation, a well-marked deep groove/fossa is present in medial view, marking the origin of the *M. pronator quadratus* (Fig. 9M).

Manus (Autopodium)—Unlike other candidodontids known so far, which do not have well-preserved autopodium elements, *Thilastikosuchus* has partially complete left and right hands (Figs. 9A, B, C, 10). A fracture extends through the distal portion of the ulna, radius, and proximal carpals (radial, ulnar, and pisiform), causing the partial loss of these regions and/or elements. However, all five metacarpals are present and articulated with each other. Additionally, digits I and II are complete,

with a phalangeal formula of 2–3 with curved unguis phalanges that are lateromedially compressed.

The proximal carpals, although partially preserved, articulate to the distal region of the ulnar. The ulnar is positioned directly above metacarpals I and II, while the radial is located near metacarpals II, IV, and V. The pisiform consists of a small semi-rounded and slightly dorsoventrally flattened ossification, with a possible neurovascular foramen developing in a posterior recess.

The metapodials have triangular proximal articular processes in anterior view, while their diaphyses have lengths and widths inversely proportional, and well-developed distal articular condyles. They are arranged in succession, with the proximal articular process of MC I overlapping MC II and so on (Fig. 10A, B). The articulation between elements occurs at the proximal portion, through ventrally concave medial projections that fit into convex surfaces on the sides of the lateral portion of the epiphysis of the subsequent element, resulting in a serial arrangement. Unlike other known notosuchians with preserved autopodial elements, the longitudinal crests separating the articulation areas in the proximal region in anterior/dorsal view are poorly developed (Sertich & Groenke, 2010; Turner, 2006).

The MC I is the most robust metapodial (Fig. 10A, B). It is short proximodistally, with a thick diaphysis and an elliptical cross section, possessing a well-developed trochlea at the distal end, marked by a semicircular medial depression separating the articular condyles, which are approximately symmetrical.

MC II is the longest metacarpal (Fig. 10A, B), with a wider proximal process and trochlea. The diaphysis is flattened. There is also observed, due to the truncation of the metapodial elements, a twist/rotation of the proximal articular portion in relation to the trochlea, in order to compensate for the inclination generated by the joint. This rotation is more pronounced in MC III, IV, and V (Fig. 10A, B), with marked elongation and thinning of the diaphysis, making them more slender elements than the medial ones.

As mentioned above, only digits I and II have all phalanges preserved (Fig. 10A, B), with the latter still articulated, but with a strong posterior inflection. The proximal phalanx of the first digit is elongated and has a mediolaterally constricted proximal metaphysis, with an anterior curvature of the diaphysis, generating a concave palmar surface. The trochlea is expanded transversely and has asymmetrical condyles, with the medial one being larger and more anteriorly projected than the lateral one, forming an inclined articular surface that also extends to the proximal facet of the unguis phalanx, which is displaced in relation to the main axis.

Unguis phalanx I is the largest among terminal phalanges, characterized by a laterally compressed blade and a concave palmar facet, acquiring a curved appearance, as in extant archosaurs (Romer, 1956). Its lateral and medial surfaces have a longitudinal groove, consistent with the blood supply that fed a keratin covering.

The second digit has three phalanges (Fig. 10A, B), including the unguis, also showing a claw-like shape. The most proximal one is higher dorsoventrally and has a transversely expanded proximal region to accommodate the articulation of MC II, followed by a morphologically similar second phalanx that is smaller and has a more curved medial margin than the lateral one (Fig. 10A, B). The unguis phalanx of the second digit, is smaller and similar to the first one, including the inclined articulation in relation to its longitudinal axis.

MC III is more elongated proximodistally than MC I and II (Fig. 10A, B) and, like the latter, also has nearly symmetrical condyles. The first phalanx follows the pattern of its equivalent in digit II, being dorsoventrally taller than the metacarpal to which it articulates, with a constricted diaphysis and proximal

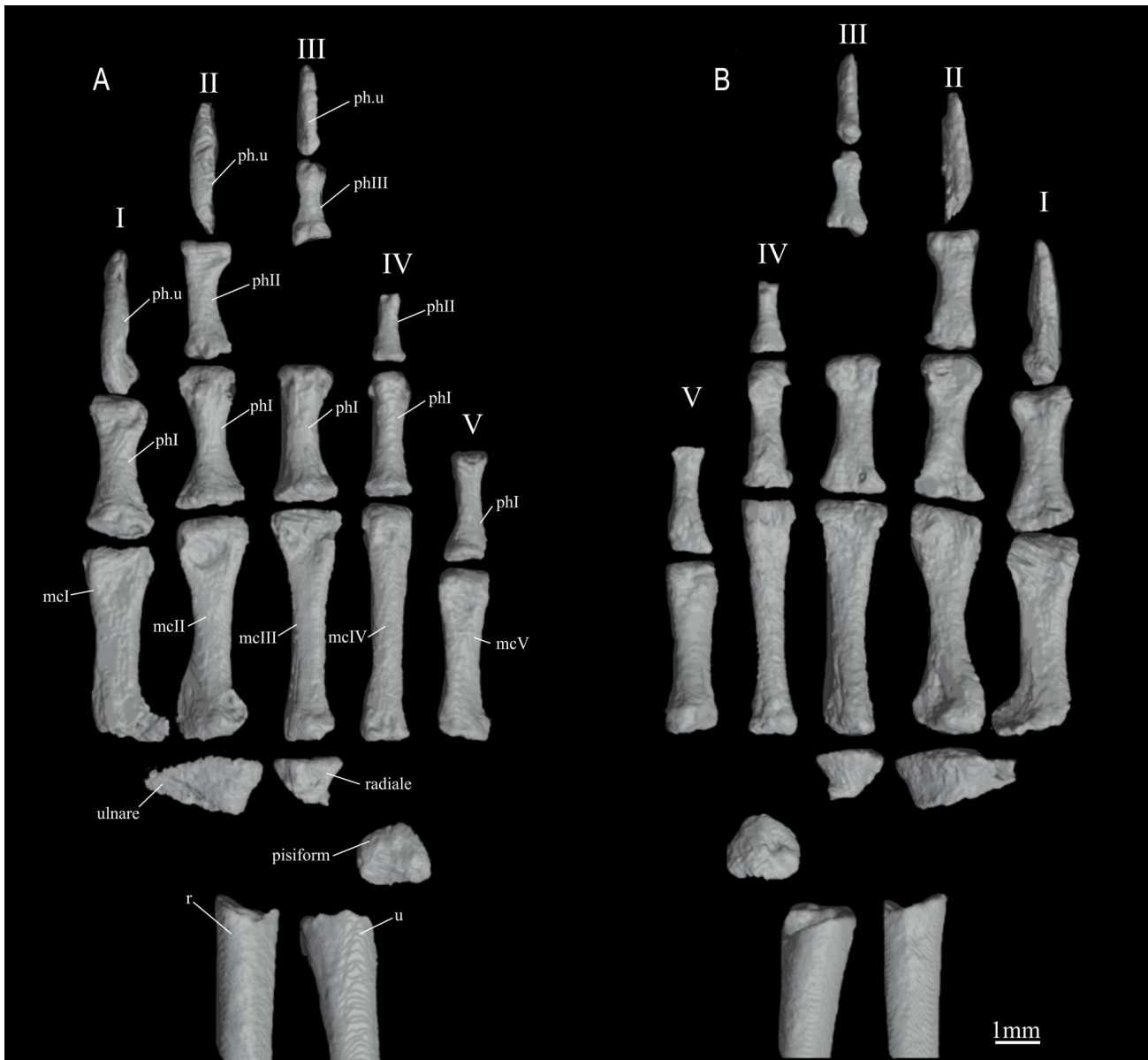


FIGURE 10. 3D segmentation of the right manus elements of *Thilastikosuchus scutoangularis*, (FUP-Pv 000019). Dorsal (A) and palmar (B) views. **Abbreviations:** mc, metacarpal; ph, phalanges; ph.u, unguinal phalanges; r, radius; u, ulna; I, II, III, IV, and V, digit numbers. Scale bar equals 1 mm.

and distal portions expanded with similar dimensions. Unfortunately, this digit is incomplete, as the second phalanx is not preserved. Nonetheless, the third and fourth (ungual) phalanges are present and preserved close to each other. The third phalanx is minute and more dorsoventrally flattened when compared with the posterior ones, but its proximal and distal epiphyses are partially eroded. The terminal phalanx of the third digit also consists of a mediolaterally compressed, ventrally curved claw with an articulation displaced from its main extension but, in this case, substantially smaller than the unguinal phalanges of digits I and II.

The fourth digit is formed by an elongated metacarpal (Fig. 10A, B), marked by a smoother transition between the diaphysis and proximal and distal ends. Only the proximal phalanx is preserved, being shorter and presenting a ventral inflection of the metaphysis that follows the proximal concavity of articulation.

The fifth digit (Fig. 10A, B) is in complete with only one phalanx. It is characterized by its more tubular appearance,

with straight diaphysis and a subtle lateral constriction and/or transverse expansion of the ends. Its metacarpal, the MC V, is the shortest in the series and has the highest level of rotation of the proximal portion relative to the trochlea.

It is necessary to emphasize the level of uncertainty regarding the phalangeal formula not only of *T. scutoangularis* but also in other notosuchians, which rarely have well-preserved autopods (Nascimento & Zaher, 2010; Sertich & Groenke, 2010; Turner 2006). Despite their conservative potential in tetrapod lineages, living crocodylians present relevant interspecific discrepancies in their phalangeal formulas, even when closely related, and there is not necessarily a direct relationship between the number of ossification centers during ontogeny and the fixed number of phalanges in maturity (Gregorovičová et al., 2018; Romer, 1956; Vieira et al., 2016). Therefore, caution is needed when extrapolating a fixed number for notosuchians based on complete specimens, as it is not always possible to determine

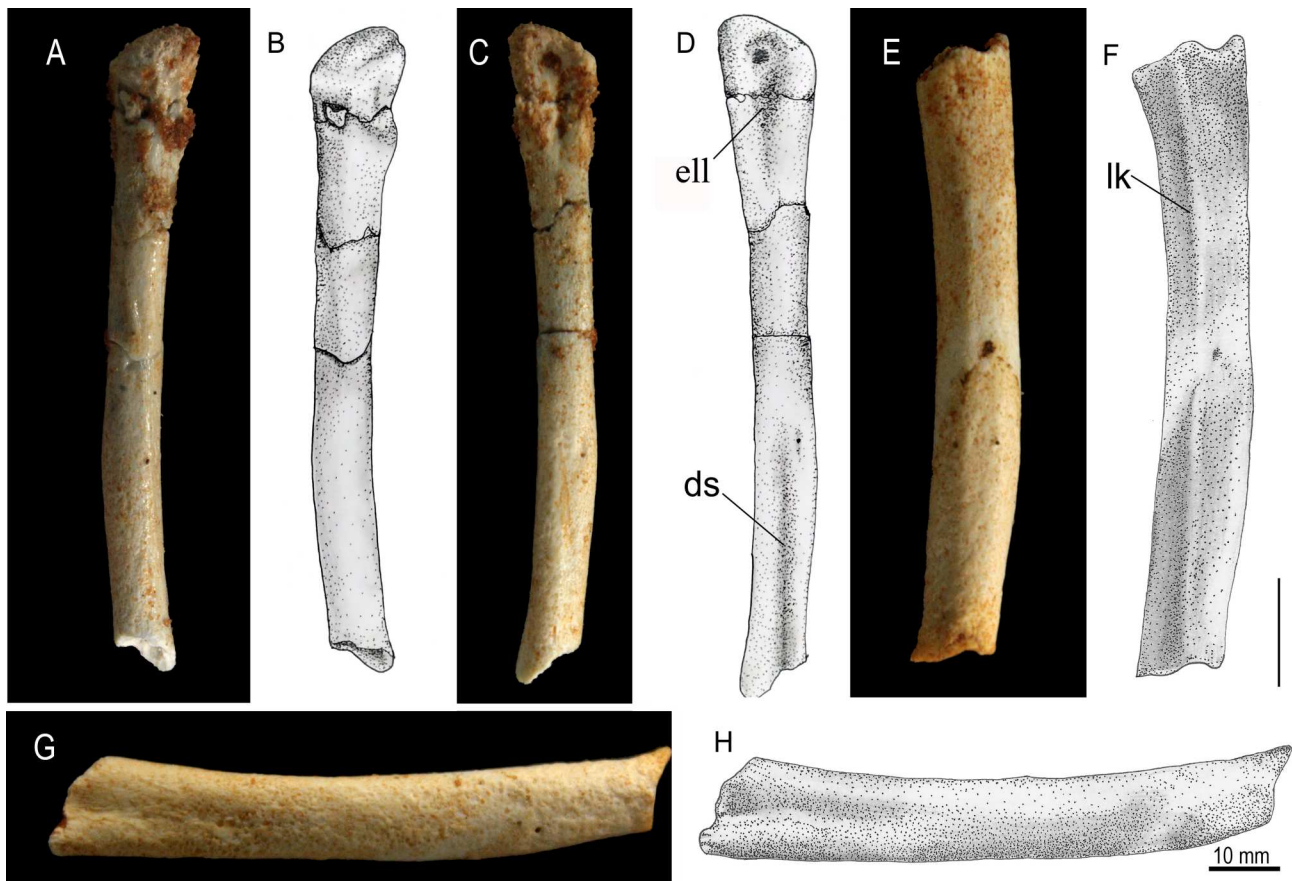


FIGURE 11. *Thilastikosuchus scutorectangularis*, (FUP-Pv 000019). A–D, right fibula in medial (A, B) and lateral (C, D) views; E–H, right tibia in lateral (E, F) and medial (G, H) views. **Abbreviations:** ds, distal sulcus; ell, external lateral ligament; lk, longitudinal keel. Scale bar equals 10 mm.

the completeness/incompleteness with a reasonable level of confidence.

Femur—The femur is badly damaged and represented only by part of the diaphysis. It has a rounded cross section, measuring 3.5 mm, being 20.6% larger in diameter than the humerus.

Incomplete Appendicular Elements (Tibia and Fibula)—Two additional long elements were found dispersed in the matrix a few centimeters away from the rest of the material. The first consists of an elongated and roughly rectilinear diaphysis, though locally bulged close to its distal end, being marked by an inferred mediolaterally flattened and slightly posteriorly bent proximal epiphysis with a somewhat flared outer margin (Fig. 11A–D). Despite not being well-preserved, these characteristics are consistent with it being a right fibula. The lateral surface of its proximal end possesses a conspicuous vertical sulcus, likely to have received the lateral ligament (ell). On its anterior margin, a minor tuberosity may relate to the iliofibularis trochanter, but it is not well-defined enough to provide robust support for this identification.

The lack of recognizable features on the second element hindered comprehensive inferences. It is fragmented and lacks both proximal and distal epiphyses. However, it displays a longitudinal low-relief crest that extends along the diaphysis, as well as a vertical and broad sulcus close to one of its extremities. There is a possibility that these comprise a tibial lateral crest and posterior depression that separates lateral and medial proximal articular facets of a tibia (Fig. 11E–H). Although not undisputed, these would be compatible with the overall relative thickness of the element.

Osteoderms—Preserved osteoderms belong to the dorsal (Fig. 6C, D, F, G) and caudal (Fig. 7C, D) portions. Some caudal osteoderms are disarticulated and scattered around the caudal vertebrae. Dorsal osteoderms clearly form two rows of parasagittal bony plates, each one associated with its dorsal vertebra. They differ morphologically from the caudal ones by being characteristically rectangular in shape, with no criss-cross pattern on their ventral surface (Fig. 6C, D, F, G). The medial edge is straight, indicating that the two parasagittal rows were connected medially to each other. The edges of anterior and posterior margins are also straight and parallel to each other (Fig. 12), giving to the element a rectangular shape. The lateral margin is smoothly rounded in the latero-anterior portion and has a small projection on the latero-posterior edge. There is an incipient ornamentation on the external surface, forming small depressions and shallow grooves. However, since the material consists of a not fully grown individual, it is not known whether this poorly developed ornamentation pattern is a feature of this species or refers only to the ontogenetic development of this individual. A poorly developed sagittal crest is present on the dorsal surface, being displaced to the lateral edge of the dermal scute (Fig. 6C, D, F, G). The sagittal crest is not present on the anterior portion of the osteoderm since each subsequent osteoderm overlaps the previous one in this area.

The more anterior and middle caudal osteoderms have a square contour (Fig. 7C, D) and their inner surface lacks the criss-cross pattern as in thoracic dermal plates. The lateral edge of the caudal dermal plates is straight, and the sagittal crest is

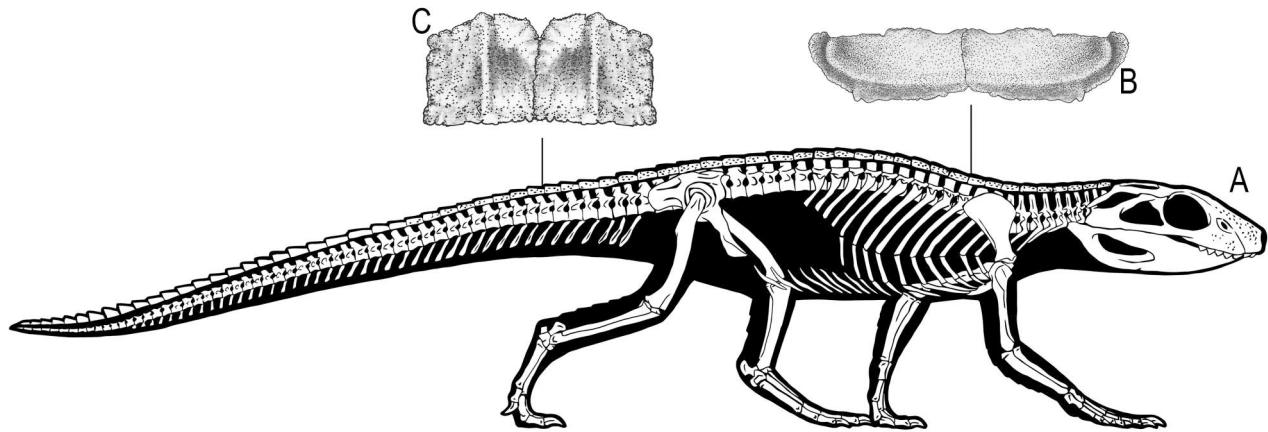


FIGURE 12. *Thilastikosuchus scutorectangularis*, (FUP-Pv 000019). **A**, skeleton reconstruction in lateral view (by Felipe Alves Elias); **B**, articulated dorsal dermal plates; **C**, articulated caudal dermal plates.

sharper and more developed. The sagittal crests divide the osteoderm into two nearly equal parts instead of being displaced to the lateral edge like in the dorsal plates. The crests do not develop on the anterior edge, indicating an overlapping pattern. In the more distal caudal plates, the crests are shorter and less sharp than in the anterior ones.

PHYLOGENETIC ANALYSIS

The phylogenetic analysis yielded 1440 most parsimonious trees (MPTs) with 1704 steps (CI=0.308 and RI=0.745) (Supplementary Files 2–4). *Gracilisuchus* was used as outgroup. Most significant is the recovery of the Candidodontidae as a monophyletic group depicted as the sister clade of all other notosuchians in the strict consensus topology. This result was only obtained through the exclusion of highly incomplete taxa (e.g., *Coringasuchus*, *Microsuchus*, *Neuquensuchus*, *Pabwehshi*, and *Pehuenchesuchus*, following the protocol used by Fiorelli et al. [2016]). *Chimaerasuchus paradoxus* was also excluded from the analysis after the revision of its coding, since it caused polytomies among many groups as well.

The overall topology of Notosuchia is distinct from those obtained by Pol et al. (2012, 2014), Leardi et al. (2015a and b), Fiorelli et al. (2016), Martin and De Broin (2016), and Martinelli et al. (2018), as *Libycosuchus* and *Simosuchus* diverge before the most recent common ancestor between the so-called Sphagesauria and Sebecosuchia (Fig. 13). Alternative datasets do not include all the possible candidodontid taxa in their analyses, like *Lavocatchampsia*, and, similarly to data matrices derived from Pol et al. (2012), generally fail to recover their monophyly, returning a paraphyletic Candidodontidae with its characteristic taxa branching at different nodes before the last common ancestor of Baurusuchidae and Sphagesauridae (Geroto & Bertini, 2019; Martins et al., 2024; Pinheiro et al., 2018, 2021).

In the present work, Candidodontidae is retrieved as the earliest diverging lineage within Notosuchia, with *Candidodon itapeturuense* as a sister taxon to the subclade composed of the remaining species. The latter is marked by a dichotomy between *Lavocatchampsia* and *T. scutorectangularis* and the clade that includes *Pakasuchus kapilimai* and *Malawisuchus mwakasyungutiensis*. The synapomorphies that support the clade are the following (as listed in the SI): 76 (insertion area for *M. pterygoideus posterior* not extending to the lateral surface of the angular (0)); 106 (four premaxillary teeth—not observed in *T. scutorectangularis* and *Lavocatchampsia* (1)); 186

(posterior process/peg on the posterior edge of the mandibular symphysis (1)); 361 (palatine width at the level of the anterior end of the suborbital fenestra about half the width of the maxillary palate); 388 (little or no variation in denticle size along denticulate ridges (0)).

After the divergence of Candidodontidae, as in other works (Bravo et al., 2021; Cunha et al., 2020; Martinelli et al., 2018), a close phylogenetic relationship was recovered between Uruguay-suchidae and the group comprising Mahajangasuchidae and Peirosauridae, whose common ancestor forms a dichotomy with Ziphosuchia. As mentioned above, the phylogenetic relationships within Ziphosuchia slightly diverge from previous articles, since *Libycosuchus* and *Simosuchus* are not closely related to Sphagesauria. Interestingly, these are also more closely related to each other, forming a small clade that includes *Llanosuchus*, *Morrinhosuchus*, and *Notosuchus*, diverging before the others. The topology of Sphagesauridae and related taxa, remains the same, marked by the presence of small sphagesaurids (*Adamantinasuchus*, *Yacarerani*, and the genus *Caipirasuchus*) and large sphagesaurids (*Sphagesaurus*, *Armadillosuchus*, and *Caryonosuchus*). Finally, baurusuchids and sebecids, unlike Sebecia, classically recovered as a monophyletic group by Larsson and Sues (2007) and more recently by Martins et al. (2024), comprise Sebecosuchia.

DISCUSSION

Morphological Comparisons with Correlate and Similar Taxa

Thilastikosuchus scutorectangularis, as a candidodontid, is part of one of the first radiations within Notosuchia. The presence of both plesiomorphic and derived characteristics warranted comparisons not only with closely related taxa, such as *Candidodon*, *Malawisuchus*, *Pakasuchus*, and *Lavocatchampsia* (Carvalho, 1994; Gomani, 1997; Martin & De Broin, 2016; O'Connor et al., 2010), but also with more derived heterodont notosuchians, such as *Morrinhosuchus*, *Notosuchus*, *Mariliasuchus*, *Yacarerani*, *Adamantinasuchus*, *Armadillosuchus*, and *Caipirasuchus* (Fiorelli & Calvo, 2008; Iori & Carvalho, 2011; Iori et al., 2018; Novas et al., 2009; Pol et al., 2014; Zaher et al., 2006).

The cranial anatomy of *T. scutorectangularis* mainly resembles other candidodontids to various degrees, while also differing from these taxa in relevant characters, some of which are interpreted here as autapomorphies that support

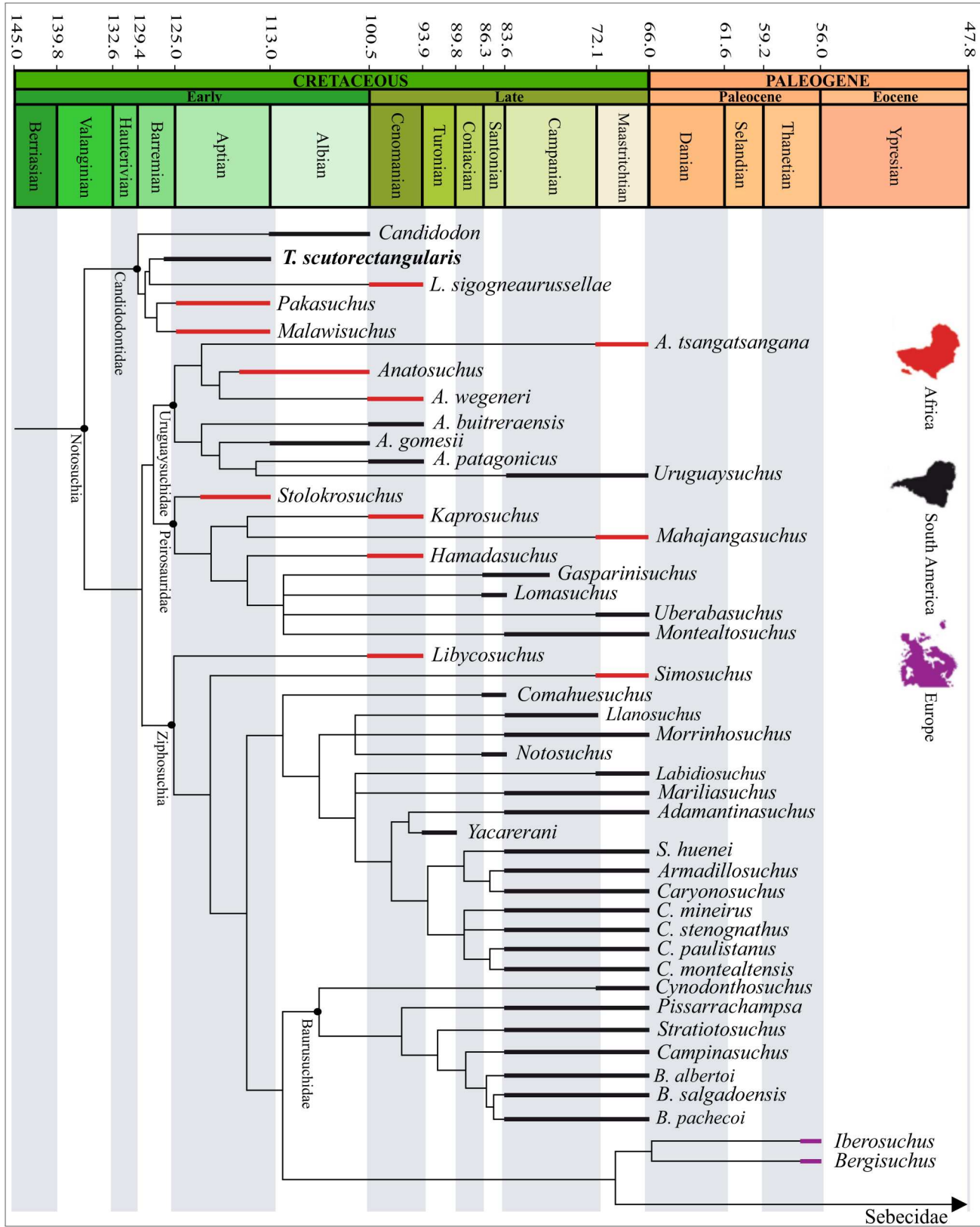


FIGURE 13. Phylogeny based in the Fiorelli et al. (2016) data matrix, modified from Pol et al. (2014), now including the specimen *Thilastikosuchus scutorectangularis*, using ordered characters (most updated version from Cunha et al., 2020). Calibrated strict consensus tree of 1440 most parsimonious trees of 1704 steps each (CI = 0.308 and RI = 0.745).



FIGURE 14. Life reconstruction of *Thilastikosuchus scutorectangularis*, Quiricó Formation (Lower Cretaceous), Sanfranciscana Basin, Minas Gerais. Artwork by Felipe Alves Elias.

the proposal of a new species. Due to the incompleteness of *L. sigogneaurussellae*, only its rostral portions and mandibular symphysis could be compared.

Thilastikosuchus scutorectangularis, *Malawisuchus*, and *Pakasuchus* share a general triangular shape of the skull in dorsal view, marked by being transversely wide in the posterior region and narrower along the rostrum, with a gradual transition between the two portions. Nonetheless, *Pakasuchus* and *T. scutorectangularis* have more laterally arched jugals than *Malawisuchus*, which has more straight lateral portions (Gomani, 1997). All candidodontids exhibit dorsoventrally flattened frontals and parietals with little lateral constriction and without a sagittal keel. The cranial roofs are rectangular, with acute lateroposterior squamosal processes and relatively small elliptical supratemporal fenestrae, with laterally inclined anterior ends and lateroposteriorly developed fossae.

The parietals in these taxa, except for *Pakasuchus*, since this portion is covered by sediment in the holotype, and *L. sigogneaurussellae*, where it is not preserved, are fused, flattened, and are composed of relatively wide skull roof elements. Their lateral margins are slightly concave and considerably thicker, bordering the supratemporal fenestrae. Unlike *T. scutorectangularis* and *Pakasuchus*, there is a significant posterior advancement of the supratemporal fossa over the squamosals in *Malawisuchus* (as also observed in MAL-49, Turner & Sertich, 2010:fig. 2C). The frontal-parietal complex in Sphagesauridae and related taxa is distinct from the pattern seen in Candidodontidae, marked by prominent sagittal crests on the

frontals and lateromedially restricted parietals (Martinelli et al., 2018; Nobre & Carvalho, 2006). While both *T. scutorectangularis* and *Malawisuchus* have a “v”-shaped suture between the frontal and parietal bones, this characteristic could not be determined for *Pakasuchus* and *Candidodon*.

The degree of contribution of the supraoccipital to the cranial roof differs between candidodontid species and is often difficult to determine. Nevertheless, in *Pakasuchus*, it appears to assume a more restricted crescent shape, while in *Malawisuchus* and *T. scutorectangularis* it has a more regular and rectangular shape, being visibly overlapped by the squamosal and parietal bones at its margins, resulting in a slightly depressed element compared with the rest of the cranial roof (Gomani, 1997: plate 2; O’Connor et al., 2010: fig. 1A; Turner & Sertich, 2010: fig. 2C). Considering only this last element, *T. scutorectangularis* differs significantly in the development of the vertical bulge of the supraoccipital, which is more robust than in *Pakasuchus* and *Malawisuchus*, accompanied by adjacent depressions on the occipital facet (autapomorphy).

The antorbital fenestra is a plesiomorphic condition in crocodyliforms (Colbert et al., 1951), with a heterogeneous distribution, not necessarily appearing to be related to any specific evolutionary signal. It is absent in *Pakasuchus*, as well as in *Libycosuchus* (Ibrahim et al., 2020), and also absent or reduced in non-sphagesaurid Sphagesauria, such as *Mariliasuchus* and *Morrinhosuchus* (Iori et al., 2018; Zaher et al., 2006). This state contrasts with its presence in *T. scutorectangularis*, *Malawisuchus*, and *Candidodon*, among

early diverging notosuchians, as well as in the small-bodied sphagesaurid genus *Caipirasuchus* (Iori & Carvalho, 2011; Martinelli et al., 2018; Pol et al., 2014).

Although often recovered in basal positions as stem-ziphosuchians or early-branching sphagesaurs (Bravo et al., 2021; Martinelli et al., 2018; Pol et al., 2014), *Libycosuchus* and *Candidodon* do not resemble the aforementioned taxa to the same degree and have considerable cranial differences from *T. scutorectangularis*. *Candidodon* has a similar overall cranial morphology to *T. scutorectangularis*, as discussed above, mainly in the architecture of the cranial roof and palate, but exhibits a distinct pattern of dermal ornamentation, marked by large and pronounced pits, as well as a hypertrophied and laterally compressed maxillary caniniform, also seen in *Pakasuchus* (Carvalho, 1994; O'Connor et al., 2010). This discrepancy in ornamentation development may be due to the ontogenetic stage of the specimen described here. *Libycosuchus* has a more oreinirostral cranial shape, an anteroposteriorly shorter cranial roof, and a large circular supratemporal fenestra (Ibrahim et al., 2020). In addition, this taxon has anteriorly positioned choanae and preserves no dentition, making it difficult to evaluate whether it had the same degree of heterodonty seen in related forms (Ösi, 2014).

The ectopterygoids and pterygoids of *T. scutorectangularis* form a single continuous surface without the development of visible pits and/or fenestrae, a condition shared by other candidodontids (Gomani, 1997; Nobre & Carvalho, 2002) and by *Morrinhosuchus* (Iori et al., 2018), but distinct from the fenestrated surfaces adjacent to the choanae in *Caipirasuchus* (Martinelli et al., 2018), which widen the margins of the internal nostrils. However, while having solid pterygoid wings, in *Malawisuchus* these are more anteroposteriorly restricted than in related species (Gomani, 1997; Ösi, 2014).

The distance between the basicranium (ventral portion of the basioccipital and basisphenoid) and the posterior margin of the pterygoids, previously discussed for sphagesaurids by Dias et al. (2020), also varies among these taxa and has potential phylogenetic value. *Thilastikosuchus scutorectangularis* bears these features in a compact organization, with little or no distance between the two portions, similar to what is seen in *Candidodon* and *Libycosuchus*. Other taxa, such as *Malawisuchus*, *Morrinhosuchus*, *Mariliasuchus*, and *Yacararani*, have conspicuous “v”-shaped notches at the bases of the pterygoids, creating an impression of anterior displacement (Iori et al., 2018; Ösi, 2014; Zaher et al., 2006). In most Sphagesauridae, these notches are also present, but to a lesser extent, except for *Caipirasuchus stenoganthus* (Pol et al., 2014).

Similarly to the skull, the symphysis and mandibular rami of *T. scutorectangularis* share characteristics with both stem-sphagesaurids and crown-group forms. Starting from the posterior portion, the external mandibular fenestrae (emf) of *T. scutorectangularis* are markedly elliptical and positioned posteriorly in the mandibular rami in lateral view and, similar to *Malawisuchus* and *Pakasuchus*, are bordered on the posterior edge by an upward projection of the angular that overlaps the surangular locally (Gomani, 1997; O'Connor et al., 2010). This small process is absent in non-sphagesaurid sphagesaurs that have preserved mandibular rami, such as *Notosuchus*, *Morrinhosuchus*, *Mariliasuchus*, and sphagesaurids in general (Zaher et al., 2006; Fiorelli & Calvo, 2008; Iori et al., 2018; Martinelli et al., 2018).

Among early-branching notosuchians, only *Libycosuchus*, *Lavocatchamps*, and *Malawisuchus* have their mandibular symphyses preserved and/or illustrated in publications. *Libycosuchus* diverges from other forms by having a short symphysis with a strong medial arching of the mandibular rami, resulting in a “u”-shaped profile in dorsal/ventral view (Ibrahim et al., 2020:fig. 77D, E). *Lavocatchamps* and *Malawisuchus* share an anteroposterior lengthening of the symphysis and significant participation of the splenials in the same way as *T. scutorectangularis* (which

reaches 40% of the total symphyseal length). However, the latter has a greater degree of deflection of the mandibular rami in relation to the sagittal plane, accentuating its “y”-shape profile, in addition to the development of a posterior symphyseal protuberance in the suture, generating two local lateral concavities, which are autapomorphic characters for *T. scutorectangularis*. Lateral symphyseal crests relative to the medial suture are absent in *T. scutorectangularis* and are potentially autapomorphic for *L. sigogneaurussellae* (Martin & De Broin, 2016). While accurately determining these characteristics in *Malawisuchus* is challenging, the specimen MAL-49 (Ösi, 2014: fig. 13B) seems to have similar structures.

The aforementioned length of the mandibular symphysis and the degree of inflection of mandibular rami in relation to the sagittal plane are crucial features for understanding the evolution of oral processing in sphagesaurids and related forms, becoming important synapomorphies that support the clade (Sphagesauria *sensu* Ruiz et al., 2021). However, this general configuration, together with heterodonty and oblique tooth implantation, is not exclusive to them, having evolved also in “Protosuchia,” such as *Edentosuchus tienshanensis* from the Lower Cretaceous of China and the undescribed Kayenta form from the Lower Jurassic of the U.S.A. (Pol et al., 2004; Ösi, 2014). Despite this, and accepting the most recent topologies (Martinelli et al., 2018; Cunha et al., 2020), a pattern of progressive increase in the symphysis suture length and inflection of its rami can be observed towards Sphagesauridae. In this context, this progression is evolutionarily informative, but it is always necessary to consider the possibility of convergence with older lineages.

There are no caniniform teeth in *T. scutorectangularis*, as is also the case in *L. sigogneaurussellae*, which differs from the condition observed in other candidodontids (*Candidodon*, *Malawisuchus*, and *Pakasuchus*), where caniniform teeth are well-developed and located in the maxilla. It should be noted that in some sphagesaurid species, the caniniform teeth are well-developed, but located in the premaxilla instead (e.g., *Yacararani*, *Caipirasuchus paulistanus*, *C. stenognathus*, *C. mineirus*, and *C. montealtensis*). Likewise, in the sphagesaurid lineage, some species also display caniniforms in the premaxilla, as observed in *Adamantinasuchus*, *Armadillosuchus*, *Mariliasuchus*, and *Notosuchus*.

The molariform teeth are multicuspid, oval-shaped, bear a “sagittal” crest in occlusal view, and are oriented obliquely in relation to the dental row, features shared with *L. sigogneaurussellae* and *Malawisuchus*. The morphology of the cingulum and the number of accessory cusps vary along the dental line. The cingulum has numerous small accessory cusps arranged around the base of the tooth crown, as observed in the species *L. sigogneaurussellae*, *Candidodon*, and *Malawisuchus*. These have complex dental morphology, different from *Chimaerasuchus paradoxus*, due to the absence of multiple rows of tubercles (Wu et al., 1995; Wu & Sues, 1996), and is also distinct from Sphagesauridae and *Notosuchus terrestris*, which have molariform teeth with a drop-shaped transverse section (Lecuona & Pol, 2008; Pol et al., 2014), and *Simosuchus clarki*, which has leaf-shaped teeth (Buckley et al., 2000).

Similarly to *T. scutorectangularis*, *L. sigogneaurussellae*, *Candidodon*, and *Malawisuchus* have distinct crowns on molariform teeth, cingular cusps, single-rooted teeth, and a medially depressed root. However, the lingual cingular cusps on posterior molariform teeth are poorly developed (or absent) in *Malawisuchus* and *T. scutorectangularis*. The first maxillary teeth have single cusps in *T. scutorectangularis*, *L. sigogneaurussellae*, and *Candidodon*, while *Malawisuchus* (see Ösi, 2014:fig. 13) has multicuspid teeth. *Candidodon* does not have striated incisiform teeth (Carvalho, 1994:fig. 5), and the first four molariform teeth are of the same size, while *Malawisuchus* has striated upper incisiform teeth and variable sizes of molariform teeth. All

longitudinal cusps in *Chimaerasuchus* extend to the anterior end of the tooth (Wu et al., 1995:figs. 1d, 2b), a condition that is not present in *Malawisuchus*.

Naturally, the distinct heterodont dentition of these forms warrants discussion on possible dietary inferences. The biomechanical implications of this morphology, in conjunction with different variations in heterodonty, were discussed in detail by Ösi (2014), revealing difficulties in directly attributing this state to herbivory, varying from case to case. Melstrom and Irmis (2019), using an extensive database, mapped dental and feeding diversity within Crocodylomorpha, pointing to both herbivory and omnivory for these heterodont lineages, while recent studies of dental histology and coprolite inclusions appear to support herbivory for sphagesaurids (Oliveira et al., 2021; Ricart et al., 2021). Thus, despite the difficulties in inferring diets directly from dental morphology, the assessed heterodont forms similar to *T. scutorectangularis* have more commonly been attributed to at least partially herbivorous diets. This, in turn, may help expand our understanding of the morphological and dietary diversity of South American notosuchians, which already seem to have exhibited a certain degree of disparity already in the Early Cretaceous.

The postcranial skeleton of *T. scutorectangularis* has significant morphological variations compared with other notosuchians. Some postcranial elements are highly fragmented, making comparison with other specimens difficult, such as the scapula and humerus, which have fragmented articulation facets. In general, the postcranial skeleton of *T. scutorectangularis* presents a typical structure of other notosuchians. The ulna of *T. scutorectangularis* has an olecranon process with a rectangular shape (Fig. 9M, N), similar to *Yacarerani boliviensis*, *Notosuchus terrestris*, and *Simosuchus clarki*. However, it differs from them by being displaced in relation to the main axis of the diaphysis. The proximal end of the ulna in *T. scutorectangularis* has two processes, an anterior and an anterolateral, as observed in other notosuchians (e.g., *Notosuchus*, *Simosuchus*, *Sebecus icaeorhinus*, *Striatotosuchus*, and *Baurusuchus albertoi*). Ventral to the olecranon process, there are muscle attachment marks for the *M. triceps brevis*, and a longitudinal groove for the insertion of the *M. extensor carpi radialis brevis* dorsally and the *M. flexor ulnaris* ventrally (Fig. 9M, N), similar to what can be seen in recent crocodylians and *Simosuchus* (Meers, 2003; Sertich & Groenke, 2010). Although not fully preserved, in the distal portion, a well-marked deep groove/fossa is present in medial view, marking the origin of the *M. pronator quadratus*, similar to that of *Y. boliviensis* (Leardi et al., 2015b: fig. 10). The radius of *T. scutorectangularis* presents a slightly laterally curved diaphysis (Fig. 9K, L), as in *Y. boliviensis* and *Araripesuchus tsangatsangana*. The articular surface has a shallow concavity that articulates with the condyles of the humerus, like *Y. boliviensis*, *Caipirasuchus mineirus*, and *Simosuchus*.

In spite of its superficial resemblance with the general crocodylomorph condition, marked by a slender aspect and laterally compressed proximal epiphysis, the putative fibula associated with *T. scutorectangularis* differs from the morphology found in most notosuchians in several aspects. Uruguaysuchids, like *Araripesuchus* (Turner, 2006), sphagesaurids, like *Y. boliviensis* (Leardi et al., 2015b), and baurusuchids (Godoy et al., 2016) all seem to share, to varying degrees, a posteriorly inflected proximal epiphysis with a broad shallow depression for the lateral ligament, contrasting to the incipient posterior flaring with a deep, tear-shaped lateral ligament, sulcus observed in this new species. As expected, the latter state is most likely shared with *Malawisuchus* (Gomani, 1997:288; Turner, 2006:345), also a candidodontid, but this feature seems to be reminiscent of non-mesoeucrocodylian crocodyliforms, like *Protosuchus richardsoni* Brown, 1933, which displays simpler fibular proximal epiphyses (Turner, 2006). These characteristics, in addition to the unusual

rectangular osteoderms, are herein interpreted as being plesiomorphic within Crocodylomorpha and corroborate an early divergence for Candidodontidae within Notosuchia.

Considering the dermal shield of various clades of Notosuchia and other crocodyliforms, it is worth highlighting that the external morphology of the dorsal and caudal dermal shields of *Thilastikosuchus* (Figs. 6C, D, F, G, 7D, 11) are loosely similar to the character state found in the so-called “protosuchians,” including Gobiosuchidae. These forms have rectangular dorsal dermal plates, which are substantially wider than long, and have laterally displaced sagittal keels that do not reach the lateral margin, which is slightly deflected (e.g., *Protosuchus richardsoni* Colbert et al., 1951; *Orthosuchus stormbergi*, Nash 1968; Dollman et al., 2018; *Cassisuchus sanzuiami*, Buscalioni, 2017). Nevertheless, there are significant differences too, including the lack of a complex articulation process in the presently described specimen, as well as differences in ornamentation patterns. The dermal plates of *O. stormbergi*, for instance, have large, rounded pits in the surface. In contrast, the dermal plates of *T. scutorectangularis* are smooth and/or marked by shallow grooves (Fig. 11). The absence of ornamentation, however, may be related to the ontogenetic stage of the specimen.

Members of Uruguaysuchidae and Peirosauridae, despite not being closely related in most phylogenetic analyses, occasionally have dorsal osteoderms that resemble the general appearance described above. For example, *Araripesuchus* has rectangular dorsal plates (Buffetaut & Taquet, 1979; Ortega et al., 2000; Price 1959; Sereno & Larsson, 2009). Nonetheless, the ratio between the transverse and anteroposterior axes differs, making the dorsal plates of *T. scutorectangularis* more laterally elongated. These species also have dorsal plates with laterally displaced keels, but not to the same degree as seen in *T. scutorectangularis*. Peirosaurids such as *Montealtosuchus arrudacamposi* Carvalho et al., 2007, have dermal shields like *Araripesuchus*, but apparently more developed over the body.

Notosuchians related to *T. scutorectangularis*, such as *Candidodon*, *L. sigogneaurussellae*, *Malawisuchus*, and *Pakasuchus*, are marked by the absence of well-preserved and/or illustrated dermal shields, which precludes more detailed comparisons. However, dermal plates belonging to *Candidodon* described by Nobre (2004), although interpreted as contour plates and distinguished by their ornamentation, have keels that border their lateral edge. *Malawisuchus*, in turn, has a similar feature, with a single contour plate with a lateral sagittal keel and, like *Pakasuchus*, more oval-shaped caudal plates with central keels (Fig. 7D) (Gomani, 1997; O'Connor et al., 2010).

Forms closely related to Sphagesauridae, such as *Mariliasuchus amarali* Carvalho & Bertini 1999, are quite distinct in terms of dermal scute morphology when compared with *T. scutorectangularis*, being rounded in superficial view with a central sagittal keel and auxiliary transverse crests (Nobre & Carvalho, 2013). Sphagesaurids have distinct osteoderm morphology, with large-bodied forms like *Armadillosuchus* having highly cohesive cervical and dorsal shields where parasagittal rows of plates are sutured together, while smaller species like *Caipirasuchus mineirus*, for example, has a single double row with individual elliptical plates (Marinho & Carvalho, 2009; Martinelli et al., 2018). Similarly, baurusuchids, as reviewed by Montefeltro (2019), possessed a paired sagittal row of elliptical osteoderms with longitudinal keels, often displaced laterally or medially.

In summary, these comparisons, when viewed in their phylogenetic context, suggest that the plesiomorphic state of the dermal shield for notosuchians consisted of a double and parasagittal row of rectangular dermal plates with laterally displaced keels (Fig. 11A). Posteriorly, these plates became more quadrangular in shape along the caudal series while their keels migrated to more central positions (Fig. 11B). This state would thus have been modified by subsequent lineages of notosuchians (Fig. 13).

Systematics, Taxonomy, and Evolutionary History of Candidodontidae

The Candidodontidae clade, here composed of *Malawisuchus*, *Pakasuchus*, *Candidodon*, *Lavocatchampsa*, and *Thilastikosuchus*, has a convoluted research history. The first materials recovered date back to the late 1980s, with the naming of *Candidodon itapecuruense* Carvalho & Campos 1988, from the Itapecuru Formation, Early Cretaceous of Brazil. It was based on an isolated multicuspoid tooth, leading to its temporary classification as triconodont mammal. Later discoveries (Carvalho, 1994; Nobre & Carvalho, 2002; Nobre, 2004), including a complete cranium (UFRJ DG 114-R), firmly established *Candidodon* as a heterodont notosuchian crocodyliform. The description of *Malawisuchus*, during the same time interval, raised the possibility of a shared ancestry between the two taxa in a wider group also including *Notosuchus* and *Chimaerasuchus* (Gomani, 1997), but a proper clade name would only come later. Candidodontidae was first erected by Carvalho et al. (2004) as a sister-group to Peirosauriformes, being defined by the node as ‘the most recent common ancestor of *Candidodon* and *Mariliasuchus* and all their descendants.’ Curiously, *Malawisuchus* was then recovered within Itasuchidae, despite the vast morphological disparity between these forms.

In the light of several phylogenetic hypotheses recovering a group comprised of *Candidodon* and *Malawisuchus* (e.g., Turner & Buckley, 2008; Zaher et al., 2006), and noting the paraphyletic nature of Candidodontidae as defined by Carvalho et al. (2004), Montefeltro et al. (2009) suggested a new stem-based definition for the clade, preserving its original name, but defining it as ‘all taxa closer to *Candidodon itapecuruense* than to *Notosuchus terrestris*, *Uruguaysuchus aznarezi*, *Comahuesuchus brachybuccalis*, *Sphagesaurus huenei*, *Baurusuchus pachecoi*, and *Crocodylus niloticus*.’ This allowed the inclusion of *Malawisuchus*, as well as stabilizing the clade for future additions of new taxa. The latter work was quickly followed by O’Connor et al. (2010), who brought about the first topology recovering a monophyletic group composed of the newly described *Pakasuchus*, together with *Candidodon* and *Malawisuchus*, with the former being more closely related to *Adamantinasuchus* than the latter two taxa. This unnamed node also contained *Mariliasuchus*. More recently, Martin and De Broin (2016) described a third African candidodontid, *Lavocatchampsa sigogneaurussellae*, from the Moroccan Kem Kem Beds, and provided a phylogenetic hypothesis with a monophyletic Candidodontidae as early-branching ziphosuchians and excluding sphagesaurs like *Mariliasuchus* and *Notosuchus*.

Recent years have seen several distinct phylogenetic hypotheses regarding the monophyly of Candidodontidae and its component taxa. A monophyletic grouping is supported by Martin and De Broin (2016) and Bravo et al. (2021), whereas other studies recovered its members as consecutive sister taxa to the clade Sebecosuchia plus Sphagesauria (Pol et al., 2014; Martinelli et al., 2018). Lastly, the latest independent datasets, while not including all candidodontids, also tend to reject its monophyly, either as consecutive successive taxa to Xenodontosuchia (Martins et al., 2024; Ruiz et al., 2021), or as members of Sphagesauridae and/or its sister taxon (Pochat-Cottiloux et al., 2023).

The new configuration presented here is relevant since it places Candidodontidae as the earliest diverging group of notosuchians known to date, marking their first radiation during the Early Cretaceous in Gondwana (Barremian–Aptian). Interestingly, the *Candidodon* lineage is considered to be the oldest among candidodontids (Fig. 13); this topology, however, may be affected by the lack of a detailed description of the available specimens, especially focusing on cranial anatomy and inference/determination of the sutures between their elements. The coding of *Candidodon* becomes impaired by the absence of these details,

a challenge further exacerbated by the intense ornamentation of the dermocranium, which may be resolved in the future with the aid of techniques such as computed tomography.

Candidodontidae, one of the earliest recognizable clades of notosuchians, also has important implications for understanding the ancestral state and evolution of latter clades of notosuchians during the Cretaceous. One possibility is that the highly developed heterodonty of the group would be plesiomorphic, being reversed in latter lineages (Uruguaysuchidae, Peirosauridae, and Sebecosuchia) and retained in the Sphagesauria, culminating in Sphagesauridae. It is also possible that the common ancestor of all notosuchians was homodont, with such a state being inherited and further modified by the medium- and large-sized predators, like baurusuchids (though some early baurusuchians also display a degree of heterodonty; e.g., *Pakasuchus*, Ruiz et al., 2021) and heterodonty being a homoplasy of Candidodontidae and Sphagesauria.

Although a biogeographic analysis is beyond the scope of this work, we highlight that a close relationship between *Lavocatchampsa* and *Thilastikosuchus*, as presently recovered, is consistent with up-to-date paleogeographic reconstructions for the formation of the South Atlantic Ocean (Granot & Dymont, 2015; Carvalho, Bengston & Lana, 2016), where connections between Northwestern Africa and Northeastern Brazil still persisted before the complete opening of the Equatorial Gateway by the Late Cenomanian, possibly allowing for faunal exchange and subsequent allopatric speciation. These small-bodied notosuchians are just one instance of a wider vertebrate fauna shared by both the Quiricó Formation of Brazil and the Moroccan Kem Kem Beds that includes abelisaurid and carcharodontosaurid theropods, rebbachisaurid and titanosaurid sauropods, borioteiid lizards, as well as sarcopterygian and lepisosteiform fish (Carvalho & Santucci, 2018, 2021, 2023; Ibrahim et al., 2020).

The earliest record of a notosuchian consists of a rostrum of the taxon *Razanandrongobe sakalava* Maganuco, Dal Sasso & Pasini, 2006 from the Lower Jurassic of Madagascar (Maganuco et al., 2006), yet the most noticeable adaptive radiation of the clade occurred during the Early Cretaceous and, following the present cladogram, can be understood to have taken place in three pulses. The first one was marked by the evolution and diversification of candidodontids between South America and Africa, already in the Barremian–Aptian; the second was characterized by the emergence of the first members of the genus *Ara-ripesuchus* and the first peirosaurids (Nicholl et al., 2021) in the Albian, also between North Africa and South America; the third pulse was essentially concentrated in southeastern Brazil (Bauru Basin) in the Late Cretaceous, and is remarkable by having generated higher diversity levels than extant crocodylians, despite the relatively small geographic area that they occupied. As previously mentioned, such a pattern of notosuchian distribution attests to the retention of continental connections between South America and North Africa, at least until the Cenomanian, which is consistent with the models of the emergence of the South Atlantic, which likely proceeded from south to north (Scotese, 2014).

CONCLUSION

A second South American candidodontid with close affinities with the North African taxon *Lavocatchampsa* is here presented. The holotype of *T. scutirectangularis*, despite being most likely based on a not fully grown specimen, is in line with the skull sizes seen in *Malawisuchus*, *Pakasuchus*, and *Lavocatchampsa* (*Candidodon* being the outlier), and shares with these taxa several diagnostic features that support its assignment as a Candidodontidae. The resulting phylogenetic hypothesis depicts Candidodontidae as an early-branching clade of notosuchians.

This new phylogenetic topology for Candidodontidae seems to be congruent with their geographic (South America and Africa) and stratigraphic (mainly from Albian/Aptian age) distributions, being the oldest confirmed notosuchians from South America. The shift in the relationships of Candidodontidae within Notosuchia indicates that the inclusion of more complete taxa in phylogenetic studies involving fossils can cause significant changes in the topology of the resulting trees.

ACKNOWLEDGMENTS

The authors are grateful to the Campo Azul Municipality for invaluable support during the field trips. We also thank Adriano Mineiro and Lucila Souza for their assistance in the fieldwork. We are also grateful to Henrique Zimmermann for his help with the geological map, Patrícia F.R. Costa for drawings presented in Figs. 4, 6–9, 11, and 12, and Felipe Elias for the reconstitution of *T. scuto rectangularis*. The comments made by an anonymous reviewer, Jeremy Martin, and the editors Michael D’Emic and Pedro Godoy greatly improved an earlier version of this manuscript. JCC was supported by Coordenação de Aperfeiçoamento de Pessoal de Nível Superior (CAPES), finance code 001, and by Conselho Nacional de Desenvolvimento Científico e Tecnológico (CNPq).

AUTHOR CONTRIBUTIONS

JCC: writing—original draft, review, and editing; methodology; fossil preparation; software; validation; investigation; conceptualization; data curation; formal analysis. DMS: writing—original draft and review; collecting; methodology. RLP: writing—review and editing; funding acquisition, collecting, data curation. RMS: writing—review and editing; conceptualization; methodology; funding acquisition, collecting, fossil preparation, data curation.

DATA AVAILABILITY STATEMENT

The authors confirm that the data supporting the findings of this study are available within the article, its supplementary materials, and at <https://doi.org/10.5281/zenodo.13357095> and <http://morphobank.org/permalink/?P5622> (NEXUS file).

DISCLOSURE STATEMENT

No potential conflict of interest was reported by the author(s).

ORCID

Joyce Celerino De Carvalho  <http://orcid.org/0000-0002-9275-1164>
Daniel Martins Dos Santos  <http://orcid.org/0009-0008-9716-8753>
Ricardo Lourenço Pinto  <http://orcid.org/0000-0002-4128-8405>
Rodrigo Miloni Santucci  <http://orcid.org/0000-0002-4326-743X>

SUPPLEMENTARY FILES

Supplementary File 1.docx: Protocol and raw results of the phylogenetic analysis.

Supplementary File 2.nex: Data matrix (NEXUS file).

Supplementary File 3.tnt: Data matrix (TNT file, with 38 ordered states).

Supplementary File 4.tre: File with 1,440 MPTs found in this study.

LITERATURE CITED

- Andrade, M. B., Edmonds, R., Benton, M. J., & Schouten, R. (2011). A new Berriasian species of *Goniopholis* (Mesoeucrocodylia, Neosuchia) from England, and a review of the genus. *Zoological Journal of the Linnean Society*, 163, S66–S108. doi:10.1111/j.1096-3642.2011.00709.x
- Arai, M., Dino, R., Milhomem, P.S., & Sgarbi, G.N.C. (1995). Micropaleontologia da Formação Areado, Cretáceo da Bacia Sanfranciscana: estudo dos ostracodes e palinologia. In: Congresso Brasileiro de Paleontologia, 14, 1995. Atas, Uberaba, SBP, pp. 1–2.
- Batezelli, A., Blanco, L. A. D., & Rebelo, T. B. (2024). Changes in the stratigraphic architecture as the response to the Upper Cretaceous tectonic and climatic interplay in the Sanfranciscana Basin, Brazil. *Marine and Petroleum Geology*, 164, <https://doi.org/10.1016/j.marpetgeo.2024.106821>
- Bittencourt, J. S., Rohn, R., Gallego, O. F., Monferran, M. D., & Uhlein, A. (2018). The morphology and systematics of the clam shrimp *Platyestheria* gen. nov. *abaetensis* (Cardoso) (Crustacea, Spinicaudata) from the Lower Cretaceous of the Sanfranciscana Basin, southeast Brazil. *Cretaceous Research*, 91, 274–286. doi:10.1016/j.cretres.2018.06.016
- Bittencourt, J. S., Simões, T. R., Caldwell, M. W., & Langer, M. C. (2020). Discovery of the oldest South American fossil lizard illustrates the cosmopolitanism of early South American squamates. *Communications Biology*, 3(1), 201. <https://doi.org/10.1038/s42003-020-0926-0>
- Bravo, G. G., Pol, D., & García-López, D. A. (2021). A new sebecid mesoeucrocodylian from the Paleocene of northwestern Argentina. *Journal of Vertebrate Paleontology*, 41(3), e1979020. <https://doi.org/10.1080/02724634.2021.1979020>
- Brochu, C. A. (1996). Closure of neurocentral sutures during crocodylian ontogeny: implications for maturity assessment in fossil archosaurs. *Journal of Vertebrate Paleontology*, 16(1), 49–62. doi:10.1080/02724634.1996.10011283
- Brown, B. (1933). An ancestral crocodile. *American Museum Novitates*, 683, 1–4.
- Buckley, G. A., Brochu, C. A., Krause, D. W., & Pol, D. (2000). A pug-nosed crocodyliform from the Late Cretaceous of Madagascar. *Nature*, 405(6789), 941–944. doi:10.1038/35016061
- Buffetaut, E., & Taquet, P. (1979). Un nouveau Crocodylien mesosuchien dans le Campanien de Madagascar, *Trematochampsia oblita*, n. sp. *Bulletin de la Société Géologique de France*, S7-XXI(2), 183–188. doi:10.2113/gssgfbull.S7-XXI.2.183
- Buscalioni, A. D. (2017). The Gobiosuchidae in the early evolution of Crocodyliformes. *Journal of Vertebrate Paleontology*, 37(3), e1324459. doi:10.1080/02724634.2017.1324459
- Cabral, V. C., Mescolotti, P. C., & Varejão, F. G. (2021). Sedimentary facies and depositional model of the Lower Cretaceous Quiricó Formation (Sanfranciscana Basin, Brazil) and their implication for the occurrence of vertebrate fauna at the Coração de Jesus region. *Journal of South American Earth Sciences*, 112, 103632. doi:10.1016/j.jsames.2021.103632
- Campos, J. E. G., & Dardene, M. A. (1997b). Estratigrafia e sedimentação da Bacia Sanfranciscana: uma revisão. *Revista Brasileira de Geociências*, 27(3), 269–282. doi:10.25249/0375-7536.1997269282
- Campos, J. E. G., & Dardene, M. A. (1997a). Origem e evolução tectônica da Bacia Sanfranciscana. *Revista Brasileira de Geociências*, 27(3), 283–294. doi:10.25249/0375-7536.1997283294
- Carmo, D. A., Tomassi, H. Z., & Oliveira, S. B. S. G. (2004). Taxonomia e distribuição estratigráfica dos ostracodes da Formação Quiricó, Grupo Areado (Cretáceo inferior), Bacia Sanfranciscana, Brasil. *Revista Brasileira de Paleontologia*, 7(2), 139–149. doi:10.4072/rbp.2004.2.06
- Carvalho, I. S., & Bertini, R. J. (1999). *Mariliasuchus*: um novo Crocodylomorpha (Notosuchia) do Cretáceo da Bacia Bauru, Brasil. *Geologia Colombiana*, 24, 83–105.
- Carvalho, I. S., & Campos, D. A. (1988). Um mamífero triconodonte do Cretáceo Inferior do Maranhão, Brasil. *Anais da Academia Brasileira de Ciências*, 60(4), 437–446.
- Carvalho, I. S., & Kattah, S. S. (1998). As pegadas fósseis do paleo-deserto da Bacia Sanfranciscana (Jurássico Superior-Cretáceo Inferior, Minas Gerais). *Anais da Academia Brasileira de Ciências*, 70, 53–67.

- Carvalho, I. S. (1994). *Candidodon*: um crocodilo com heterodontia (Notosuchia, Cretáceo Inferior - Brasil). *Anais da Academia Brasileira de Ciências*, 66, 331–346.
- Carvalho, I. S., Ribeiro, L. C. B., & Avilla, L. S. (2004). *Uberabasuchus terrificus* sp. nov., a new Crocodylomorpha from the Bauru Basin (Upper Cretaceous), Brazil. *Gondwana Research*, 7(4), 975–1002. doi:10.1016/S1342-937X(05)71079-0
- Carvalho, I. S., Vasconcellos, F. M., & Tavares, S. A. S. (2007). *Montealtosuchus arrudacamposi*, a new peirosaurid crocodile (Mesoeucrocodylia) from the Late Cretaceous Adamantina Formation of Brazil. *Zootaxa*, 1607, 35–46.
- Carvalho, J. C., & Santucci, R. M. (2018). New dinosaur remains from the Quiricó Formation, Sanfranciscana Basin (Lower Cretaceous), Southwestern Brazil. *Cretaceous Research*, 85, 20–27. doi:10.1016/j.cretres.2017.12.017
- Carvalho, J. C., & Santucci, R. M. (2023). A new fossil Squamata from the Quiricó Formation (Lower Cretaceous), Sanfranciscana Basin, Minas Gerais, Brazil. *Cretaceous Research*, doi.org/10.1016/j.cretres.2023.105717
- Carvalho, J. C., & Santucci, R. M. (2021). New fish remains from the Quiricó Formation (Lower Cretaceous, Sanfranciscana Basin), Minas Gerais, Brazil. *Journal of South American Earth Sciences*, 111, 103430. https://doi.org/10.1016/j.jsames.2021.103430
- Carvalho, M. D. A., Bengtson, P., & Lana, C. C. (2016). Late Aptian (Cretaceous) paleoceanography of the South Atlantic Ocean inferred from dinocyst communities of the Sergipe Basin, Brazil. *Paleoceanography*, 31(1), 2–26. doi:10.1002/2014PA002772
- Carvalho, M. S. S., & Meisey, J. G. (2008). New occurrence of *Mawsonia* (Sarcopterygii: Actinistia) from the Early Cretaceous of the Sanfranciscana Basin, Minas Gerais, southeastern Brazil. In L. Cavin, A. Longbottom, & M. Richter (Eds.), *Fishes and the Break-up of Pangea 295* (pp. 109–144).
- Chiappe, L. M. (1988). A new trematochampsid crocodile from the Early Cretaceous of north-western Patagonia, Argentina and its palaeobiogeographical and phylogenetic implications. *Cretaceous Research*, 9(4), 379–389. doi:10.1016/0195-6671(88)90009-2
- Clark, J. M. (1994). Patterns of evolution in Mesozoic Crocodyliformes. In N. C. Fraser, & H. D. Sues (Eds.), *In the Shadow of the Dinosaurs; Early Mesozoic Tetrapods* (pp. 84–97). Cambridge University Press.
- Coimbra, J. C. (2020). The genus *Cypridea* (Crustacea, Ostracoda) and the age of the Quiricó Formation, SE Brazil: a critical review. *Revista Brasileira de Paleontologia*, 23(2), 90–97. doi:10.4072/rbp.2020.2.02
- Colbert, E. H., Mook, C. C., & Brown, B. (1951). The ancestral crocodylian *Protosuchus*. *Bulletin of the American Museum Natural History*, 97(3), 1–50.
- Cunha, G. O., Santucci, R. M., Andrade, M. B., & Oliveira, C. E. M. (2020). Description and phylogenetic relationships of a large-bodied sphagesaurid notosuchian from the Upper Cretaceous Adamantina Formation, Bauru Group, São Paulo, southeastern Brazil. *Cretaceous Research*, 106, 104259. doi:10.1016/j.cretres.2019.104259
- Dias, W. A. F., Iori, F. V., Ghilardi, A. M., & Fernandes, M. A. (2020). The pterygoid region and cranial airways of *Caipirasuchus paulistanus* and *Caipirasuchus montealtensis* (Crocodyliformes, Sphagesauridae), from the Upper Cretaceous Adamantina Formation, Bauru Basin, Brazil. *Cretaceous Research*, 106, 104192. doi:10.1016/j.cretres.2019.104192
- Dollman, K. N., Clark, J. M., Norell, M. A., Xing, X., & Choiniere, J. N. (2018). Convergent evolution of a eusuchian-type secondary palate within Shartegosuchidae. *American Museum Novitates*, 3901(3901), 1–23. doi:10.1206/3901.1
- dos Santos, D. M., de Carvalho, J. C., de Oliveira, C. E. M., de Andrade, M. B., & Santucci, R. M. (2024). Cranial and postcranial anatomy of a juvenile baurusuchid (Notosuchia, Crocodylomorpha) and the taxonomical implications of ontogeny. *The Anatomical Record*, 1–46. https://doi.org/10.1002/ar.25419
- dos Santos, D. M., Santucci, R. M., Oliveira, C. E. M., & Andrade, M. B. (2022). A baurusuchid yearling (Mesoeucrocodylia, Crocodyliformes), from the Adamantina Formation, Bauru Group, Upper Cretaceous of Brazil. *Historical Biology*, 34(11), 2137–2151. doi:10.1080/08912963.2021.2001807
- Fiorelli, L. E., & Calvo, J. (2008). New remains of *Notosuchus terrestris* Woodward, 1896 (Crocodyliformes: Mesoeucrocodylia) from Late Cretaceous of Neuquén, Patagonia, Argentina. *Arquivos do Museu Nacional*, 66, 83–124.
- Fiorelli, L. E., Leardi, J. M., Hechenleitner, E. M., Pol, D., Basilici, G., & Grellet-Tinner, G. (2016). A new late Cretaceous crocodyliform from the western margin of Gondwana (La Rioja Province, Argentina). *Cretaceous Research*, 60, 194–209. doi:10.1016/j.cretres.2015.12.003
- Gasparini, Z. B. (1971). Los Notosuchia del Cretácico de América del Sur como un nuevo infraorden de los Mesosuchia (Crocodylia). *Ameghiniana*, 8, 83–103.
- Geroto, C. F. C., & Bertini, R. J. (2019). New material of *Pepesuchus* (Crocodyliformes; Mesoeucrocodylia) from the Bauru Group: implications about its phylogeny and the age of the Adamantina Formation. *Zoological Journal of the Linnean Society*, 185(2), 312–334. doi:10.1093/zoolinnean/zly037
- Godoy, P. L., Bronzati, M., Eltink, E., Marsola, J. C. D. A., Cidade, G. M., Langer, M. C., & Montefeltro, F. C. (2016). Postcranial anatomy of *Pissarrachampsia sera* (Crocodyliformes, Baurusuchidae) from the Late Cretaceous of Brazil: insights on lifestyle and phylogenetic significance. *PeerJ*, 4, e2075. doi:10.7717/peerj.2075
- Goloboff, P. A., Farris, J. S., & Nixon, K. C. (2008). TNT, a free program for phylogenetic analysis. *Cladistics*, 24(5), 774–786. doi:10.1111/j.1096-0031.2008.00217.x
- Gomani, E. M. (1997). A crocodyliform from the Early Cretaceous dinosaur beds, Northern Malawi. *Journal of Vertebrate Paleontology*, 17(2), 280–294. doi:10.1080/02724634.1997.10010975
- Granot, R., & Dymont, J. (2015). The cretaceous opening of the South Atlantic Ocean. *Earth and Planetary Science Letters*, 414, 156–163. doi:10.1016/j.epsl.2015.01.015
- Gregorovičová, M., Kvasilová, A., & Sedmera, D. (2018). Ossification pattern in forelimbs of the siamese crocodile (*Crocodylus siamensis*): Similarity in ontogeny of carpus among crocodylian species. *The Anatomical Record*, 301(7), 1159–1168. doi:10.1002/ar.23792
- Griffin, C. T., Stocker, M. R., Colleary, C., Stefanic, C. M., Lessner, E. J., Riegler, M., & Nesbitt, S. J. (2021). Assessing ontogenetic maturity in extinct saurian reptiles. *Biological Reviews*, 96(2), 470–525. doi:10.1111/brv.12666
- Ibrahim, N., Sereno, P. C., Varricchio, D. J., Martill, D. M., Dutheil, D. B., Unwin, D. M., Baidder, L., Larsson, H. C. E., Zouhri, S., & Kaoukaya, A. (2020). Geology and paleontology of the Upper Cretaceous Kem Group of eastern Morocco. *ZooKeys*, 928, 1–216. doi:10.3897/zookeys.928.47517
- Iori, F. V., & Carvalho, I. S. (2011). *Caipirasuchus paulistanus*, a new sphagesaurid (Crocodylomorpha, Mesoeucrocodylia) from the Adamantina Formation (Upper Cretaceous, Turonian–Santonian), Bauru Basin, Brazil. *Journal of Vertebrate Paleontology*, 31(6), 1255–1264. doi:10.1080/02724634.2011.602777
- Iori, F. V., Marinho, T. S., Carvalho, I. S., & Frare, L. A. S. (2018). Cranial morphology of *Morrinhosuchus luziae* (Crocodyliformes, Notosuchia) from the Upper Cretaceous of the Bauru Basin, Brazil. *Cretaceous Research*, 86, 41–52. doi:10.1016/j.cretres.2018.02.010
- Larsson, H. C. E., & Sues, H. D. (2007). Cranial osteology and phylogenetic relationships of *Hamadasuchus rebouli* (Crocodyliformes: Mesoeucrocodylia) from the Cretaceous of Morocco. *Zoological Journal of the Linnean Society*, 149(4), 533–567. doi:10.1111/j.1096-3642.2007.00271.x
- Leardi, J. M., Fiorelli, L. E., & Gasparini, Z. (2015a). Redescription and reevaluation of the taxonomical status of *Microsuechus schilleri* (Crocodyliformes: Mesoeucrocodylia) from the Upper Cretaceous of Neuquén, Argentina. *Cretaceous Research*, 52, 153–166. doi:10.1016/j.cretres.2014.09.007
- Leardi, J. M., Pol, D., Novas, F. E., & Suarez-Riglos, M. (2015b). The postcranial anatomy of *Yacarerani boliviensis* and the phylogenetic significance of the notosuchian postcranial skeleton. *Journal of Vertebrate Paleontology*, 35(6), e 995187. doi:10.1080/02724634.2014.995187
- Lecuona, A., & Pol, D. (2008). Tooth morphology of *Notosuchus terrestris* (Notosuchia: Mesoeucrocodylia): new evidence and implications. *Comptes Rendus Palevol*, 7(7), 407–417. doi:10.1016/j.crpv.2008.07.001
- Leite, A. M., Carmo, D. A., Ress, C. B., Pessoa, M., Caixeta, G. M., Denezine, M., Adorno, R. R., & Antonietto, L. S. (2018). Taxonomy of limnic Ostracoda (Crustacea) from the Quiricó Formation, Lower Cretaceous, São Francisco Basin, Minas Gerais

- State, Southeast Brazil. *Journal of Paleontology*, 92(4), 661–680. doi:10.1017/jpa.2018.1
- Lima, M.R. (1979). Palinologia dos calcários laminados da Formação Areado, Cretáceo de Minas Gerais. In: Simpósio Regional de Geologia 2. Atas, Rio Claro, UNESP, pp. 203–216.
- Maganuco, S., Dal Sasso, C., & Passini, G. (2006). A new large predatory archosaur from the Middle Jurassic of Madagascar. *Atti della Società Italiana di Scienze Naturali e del Museo Civico di Storia Naturale in Milano*, 147(1), 19–51.
- Marinho, T. S., & Carvalho, I. S. (2009). An armadillo-like sphagesaurid crocodyliform from the Late Cretaceous of Brazil. *Journal of South American Earth Sciences*, 27(1), 36–41. doi:10.1016/j.jsames.2008.11.005
- Martin, J. E., & De Broin, F. L. (2016). A miniature notosuchian with multicuspid teeth from the Cretaceous of Morocco. *Journal of Vertebrate Paleontology*, 36(6), 1211534. DOI: 10.1080/02724634.2016.1211534
- Martinelli, A. G., Marinho, T. S., Iori, F. V., & Ribeiro, L. C. B. (2018). The first *Caipirasuchus* (Mesoeucrocodylia, Notosuchia) from the Late Cretaceous of Minas Gerais, Brazil: new insights on sphagesaurid anatomy and taxonomy. *PeerJ*, 6, e5594. doi:10.7717/peerj.5594
- Martins, K. C., Queiroz, M. V. L., Ruiz, J. V., Langer, M. C., & Montefeltro, F. C. (2024). A new Baurusuchidae (Notosuchia, Crocodyliformes) from the Adamantina Formation (Bauru Group, Upper Cretaceous), with a revised phylogenetic analysis of Baurusuchia. *Cretaceous Research*, 153, 105680. doi:10.1016/j.cretres.2023.105680
- Meers, M. B. (2003). Crocodylian forelimb musculature and its relevance to Archosauria. *The Anatomical Record Part A: Discoveries in Molecular, Cellular, and Evolutionary Biology*, 274A(2), 891–916. doi:10.1002/ar.a.10097
- Melstrom, K., & Irmis, R. (2019). Repeated evolution of herbivorous crocodyliforms during the Age of Dinosaurs. *Current Biology*, 29(14), 683–685. doi:10.1016/j.cub.2019.05.076
- Montefeltro, F. C. (2019). The osteoderms of baurusuchid crocodyliforms (Mesoeucrocodylia, Notosuchia). *Journal of Vertebrate Paleontology*, 39(2), e1594242. doi:10.1080/02724634.2019.1594242
- Montefeltro, F. C., Andrade, D. V., & Larsson, H. C. E. (2016). The evolution of the meatal chamber in crocodyliforms. *Journal of Anatomy*, 228(5), 838–863. doi:10.1111/joa.12439
- Montefeltro, F. C., Laurini, C. R., & Langer, M. C. (2009). Multicusped crocodyliform teeth from the Upper Cretaceous (São José do Rio Preto Formation, Bauru Group) of São Paulo, Brazil. *Cretaceous Research*, 30(5), 1279–1286. doi:10.1016/j.cretres.2009.07.003
- Nascimento, P. M., & Zaher, H. (2010). A new species of *Baurusuchus* (Crocodyliformes, Mesoeucrocodylia) from the Upper Cretaceous of Brazil, with the first complete postcranial skeleton described for the family Baurusuchidae. *Papéis Avulsos de Zoologia*, 50, 323–361.
- Nash, D. (1968). A crocodile from the Upper Triassic of Lesotho. *Journal of Zoology*, 156(2), 163–179. doi:10.1111/j.1469-7998.1968.tb05927.x
- Nicholl, C. S. C., Hunt, E. S. E., Ouarhache, D., & Mannion, P. D. (2021). A second peirosaurid crocodyliform from the mid-Cretaceous Kem Kem Group of Morocco and the diversity of Gondwanan notosuchians outside South America. *Royal Society Open Science*, 8(10), 211254. doi:10.1098/rsos.211254
- Nobre, P.H. & Carvalho, I.S. (2002). Osteologia do crânio de *Candidodon itapecuruense* (Crocodylomorpha, Mesoeucrocodylia) do Cretáceo do Brasil. In: Simpósio Sobre o Cretáceo do Brasil, 6, 2002. Boletim, São Pedro, p. 77–82.
- Nobre, P. H., & Carvalho, I. S. (2006). *Adamantinasuchus navae*: a new Gondwanan Crocodylomorpha (Mesoeucrocodylia) from the Late Cretaceous of Brazil. *Gondwana Research*, 10(3–4), 370–378. doi:10.1016/j.jgr.2006.05.008
- Nobre, P. H., & Carvalho, I. S. (2013). Postcranial skeleton of *Mariliusuchus amarali* Carvalho and Bertini, 1999 (Mesoeucrocodylia) from the Bauru Basin, Upper Cretaceous of Brazil. *Ameghiniana*, 50(1), 98–113. doi:10.5710/AMGH.15.8.2012.500
- Nobre, P. H. (2004). Morfologia pós-craniana de *Candidodon itapecuruense* (Crocodylomorpha, Mesoeucrocodylia), do Cretáceo do Brasil. *Revista Brasileira de Paleontologia*, 7, 87–92.
- Novas, F. E., Pais, D. F., Pol, D., Carvalho, I. D. S., Scanferla, A., Mones, A., & Riglos, M. S. (2009). Bizarre notosuchian crocodyliform with associated eggs from the Upper Cretaceous of Bolivia. *Journal of Vertebrate Paleontology*, 29(4), 1316–1320. doi:10.1671/039.029.0409
- O'Connor, P. M., Sertich, J. J. W., Stevens, N. J., Roberts, E. M., Gottfried, M. D., Hieronymus, T. L., Jinnah, Z., Ridgley, R., Ngasala, S., & Temba, J. (2010). The evolution of mammal-like crocodyliforms in the Cretaceous Period of Gondwana. *Nature*, 466(7307), 748–751. doi:10.1038/nature09061
- Oliveira, F. A., Santucci, R. M., Oliveira, C. E. M., & Andrade, M. B. (2021). Morphological and compositional analyses of coprolites from the Upper Cretaceous Bauru Group reveal dietary habits of notosuchian fauna. *Lethaia*, 54(5), 664–686. doi:10.1111/let.12431
- Ortega, F., Gasparini, Z., Buscalioni, A. D., & Calvo, J. O. (2000). A new species of *Araripesuchus* (Crocodylomorpha, Mesoeucrocodylia) from the lower Cretaceous of Patagonia (Argentina). *Journal of Vertebrate Paleontology*, 20(1), 57–76. doi:10.1671/0272-4634(2000)020[0057:ANSOAC]2.0.CO;2
- Ösi, A. (2014). The evolution of jaw mechanism and dental function in heterodont crocodyliforms. *Historical Biology*, 26(3), 279–414. doi:10.1080/08912963.2013.777533
- Pinheiro, A. E. P., Souza, L. G. D., Bandeira, K. L., Brum, A. S., Pereira, P. V. L. G., Castro, L. O. R. D. & Simbras, F. M. (2021). The first notosuchian crocodyliform from the Araçatuba Formation (Bauru Group, Paraná Basin), and diversification of sphagesaurians. *Anais da Academia Brasileira de Ciências*, 93(suppl 2), e20201591. doi:10.1590/0001-3765202120201591
- Pinheiro, A. E. P., Pereira, P. V. L. G. D. C., de Souza, R. G., Brum, A. S., Lopes, R. T., Machado, A. S., & Simbras, F. M. (2018). Reassessment of the enigmatic crocodyliform “*Goniopholis paulistanus* Roxo, 1936: Historical approach, systematic, and description by new materials. *PLoS ONE*, 13(8), e0199984.
- Pochat-Cottilloux, Y., Perrier, V., Amiot, R., & Martin, J. E. (2023). A peirosaurid mandible from the Albian–Cenomanian (Lower Cretaceous) of Algeria and the taxonomic content of *Hamadasuchus* (Crocodylomorpha, Peirosauridae). *Papers in Palaeontology*, 9(2), e1485. doi:10.1002/spp2.1485
- Pol, D. (2003). New remains of *Sphagesaurus huenei* (Crocodylomorpha: Mesoeucrocodylia) from the Late Cretaceous of Brazil. *Journal of Vertebrate Paleontology*, 23(4), 817–831. doi:10.1671/A1015-7
- Pol, D. (2005). Postcranial remains of *Notosuchus terrestris* (Archosauria: Crocodyliformes) from the upper Cretaceous of Patagonia, Argentina. *Ameghiniana*, 42(1), 1–17.
- Pol, D., Leardi, J. M., Lecuona, A., & Krause, M. (2012). Postcranial anatomy of *Sebecus icaeorhinus* (Crocodyliformes, Sebecidae) from the Eocene of Patagonia. *Journal of Vertebrate Paleontology*, 32(2), 328–354. doi:10.1080/02724634.2012.646833
- Pol, D., Nascimento, P., Carvalho, M., Riccomini, A. B., Pires-Domingues, R. A., & Zaher, H. (2014). A new notosuchian from the Late Cretaceous of Brazil and the phylogeny of advanced notosuchians. *PLoS ONE*, 9(4), 93105. doi:10.1371/journal.pone.0093105
- Pol, D., S. Ji, J. M., Clark, & Chiappe, L.M. (2004). Basal crocodyliforms from the Lower Cretaceous Tugulu Group (Xinjiang, China), and the phylogenetic position of *Edentosuchus*. *Cretaceous Research*, 25(4), 603–622. doi:10.1016/j.cretres.2004.05.002
- Price, L. I. (1945). A new reptile from the Cretaceous of Brazil. *Notas Preliminares e Estudos, Serviço Geologia Mineralogia do Brasil*, 25, 1–8.
- Price, L. I. (1950). On a new crocodylian, *Sphagesaurus*, from the Cretaceous of the State of São Paulo, Brazil. *Anais da Academia Brasileira de Ciências*, 22(1), 77–83.
- Price, L. I. (1955). Novos crocodilídeos dos arenitos da Série Bauru. Cretáceo do Estado de Minas Gerais. *Anais da Academia Brasileira de Ciências*, 27(4), 487–498.
- Price, L. I. (1959). Sobre um crocodilídeo notossuquido do Cretácico Brasileiro. *Serviço Gráfico do Instituto Brasileiro de Geografia e Estatística*, 188, 56.
- Ricart, R. S. D., Santucci, R. M., Andrade, M. B., Oliveira, C. E. M., Nava, W. R., & Degrazia, G. F. (2021). Dental histology of three notosuchians (Crocodylomorpha) from the Bauru Group, Upper Cretaceous, South-eastern Brazil. *Historical Biology*, 33(7), 1012–1023. doi:10.1080/08912963.2019.1675057
- Romer, A.S. (1956). *Osteology of the Reptiles*. Chicago: University of Chicago Press, 772 pp.
- Ruiz, J. V., Bronzati, M., Ferreira, G. S., Martins, K. C., Queiroz, M. V., Langer, M. C., & Montefeltro, F. C. (2021). A new species of *Caipirasuchus* (Notosuchia, Sphagesauridae) from the Late

- Cretaceous of Brazil and the evolutionary history of Sphagesauria. *Journal of Systematic Palaeontology*, 19(4), 265–287. doi:10.1080/14772019.2021.1888815
- Scotese, R. C. (2014). Atlas of Late Cretaceous Paleogeographic Maps, PALEOMAP Atlas for ArcGIS, volume 2, The Cretaceous, Maps 16–22, Mollweide Projection, PALEOMAP Project, Evanston, IL.
- Sereno, P. C., & Larsson, H. C. E. (2009). Cretaceous crocodyliforms from the Sahara. *ZooKeys*, 28, 1–143. doi:10.3897/zookeys.28.325
- Sertich, J. W., & Groenke, J. R. (2010). The appendicular skeleton of *Simosuchus clarki* (Crocodyliformes: Notosuchia) from the Late Cretaceous of Madagascar. Society of Vertebrate Paleontology Memoir. In: Krause DW, Kley NJ, eds. *Journal of Vertebrate Paleontology*, 30 (Supplement 6), 122–153.
- Simpson, G. G. (1937). New reptiles from the Eocene of South America. *American Museum Novitates*, 927, 1–3.
- Turner, A. H., & Sertich, J. J. W. (2010). Phylogenetic history of *Simosuchus clarki* (Crocodyliformes: Notosuchia) from the Late Cretaceous of Madagascar. *Journal of Vertebrate Paleontology*, 30(sup1), 177–236. doi:10.1080/02724634.2010.532348
- Turner, A. H. (2006). Osteology and phylogeny of a new species of *Araripesuchus* (Crocodyliformes, Mesoeucrocodylia) from the Late Cretaceous of Madagascar. *Historical Biology*, 18(3), 255–369. doi:10.1080/08912960500516112
- Turner, A. H., & Buckley, G. A. (2008). *Mahajangasuchus insignis* (Crocodyliformes: Mesoeucrocodylia) cranial anatomy and new data on the origin of the eusuchian-style palate. *Journal of Vertebrate Paleontology*, 28(2), 382–408. doi:10.1671/0272-4634(2008)28[382:MICMCA]2.0.CO;2
- Vieira, L. G., Santos, A. L. Q., Lima, F. C., Mendonça, S. H. S. T., Menezes, I. T., & Sebben, A. (2016). Ontogeny of the appendicular skeleton in *Melanosuchus niger* (Crocodylia: Alligatoridae). *Zoological Science*, 32(4), 372–383. doi:10.2108/zs150130
- Walker, A. D. (1970). A revision of the Jurassic reptile *Hallopus victor* (Marsh), with remarks on the classification of crocodyles. *Philosophical Transactions of the Royal Society of London. B, Biological Sciences*, 257(816), 323–372. doi:10.1098/rstb.1970.0028
- Whetstone, K. N., & Whybrow, P. J. (1983). A ‘cursorial’ crocodylian from the Triassic of Lesotho (Basutoland), southern Africa. *Occasional Papers of the Museum of Natural History of the University of Kansas*, 106, 1–37.
- Wu, X. C., & Sues, H. D. (1996). Anatomy and phylogenetic relationships of *Chimaerasuchus paradoxus*, an unusual crocodyliform reptile from the Lower Cretaceous of Hubei, China. *Journal of Vertebrate Paleontology*, 16(4), 688–702. doi:10.1080/02724634.1996.10011358
- Wu, X. C., Sues, H. D., & Sun, A. (1995). A plant-eating crocodyliform reptile from the Cretaceous of China. *Nature*, 376(6542), 678–680. doi:10.1038/376678a0
- Yushkevich, P. A., Piven, J., Hazlett, H. C., Smith, R. G., Ho, S., Gee, J. C., & Gerig, G. (2006). User-guided 3D active contour segmentation of anatomical structures: Significantly improved efficiency and reliability. *NeuroImage*, 31(3), 1116–1128. doi:10.1016/j.neuroimage.2006.01.015
- Zaher, H., Pol, D., Carvalho, A. B., Nascimento, P. M., & Riccomini, C. (2011). A complete skull of an Early Cretaceous sauropod and the evolution of advanced titanosaurs. *PLoS ONE*, 6(2), e16663. doi:10.1371/journal.pone.0016663
- Zaher, H., Pol, D., Carvalho, A. B., Riccomini, C., Campos, D., & Nava, W. (2006). Redescription of the cranial morphology of *Mariliasuchus amarali*, and its phylogenetic affinities (Crocodyliformes, Notosuchia). *American Museum Novitates*, 2006(1), 1–40. doi:10.1206/0003-0082(2006)3512[1:ROTCMO]2.0.CO;2
- Zaher, H., Pol, D., Navarro, B. A., Delcourt, R., & Carvalho, A. B. (2020). An Early Cretaceous theropod dinosaur from Brazil sheds light on the cranial evolution of the Abelisauridae. *Comptes Rendus Palevol*, 19(1-2), 101–115. doi:10.7202/1069879ar

Handling Editor: Pedro Godoy.

Phylogenetics Editor: Pedro Godoy.